

# Multiple-scattering frequency-time hybrid solver for the wave equation in interior domains

Oscar P. Bruno\* and Tao Yin†

June 7, 2022

## Abstract

This paper proposes a frequency-time hybrid solver for the time-dependent wave equation in two-dimensional *interior spatial domains*. The approach relies on four main elements, namely, 1) A multiple scattering strategy that decomposes a given time-domain problem into a sequence of *limited-duration* time-domain problems of scattering by overlapping open-arcs, each one of which is reduced (by means of the Fourier transform) to a sequence of *Helmholtz frequency-domain problems*; 2) Boundary integral equations on overlapping boundary patches for the solution of the frequency-domain problems in point 1); 3) A smooth “*Time-windowing and recentering*” methodology that enables both treatment of incident signals of long duration and long time simulation; and, 4) A Fourier transform algorithm that delivers numerically dispersionless, *spectrally-accurate time evolution* for given incident fields. By recasting the interior time-domain problem in terms of a sequence of open-arc multiple scattering events, the proposed approach regularizes the full interior frequency domain problem—which, if obtained by either Fourier or Laplace transformation of the corresponding interior time-domain problem, must encapsulate infinitely many scattering events, giving rise to non-uniqueness and eigenfunctions in the Fourier case, and ill conditioning in the Laplace case. Numerical examples are included which demonstrate the accuracy and efficiency of the proposed methodology.

**Keywords:** wave equation, multiple scattering, Fourier transform, integral equation

**MSC:** 35L05, 65M80, 65T99, 65R20

## 1 Introduction

The numerical solution of the classical scalar second-order wave equation remains a challenging problem, with significant impact, directly and indirectly, on the simulation of propagation and scattering of time dependent acoustic, elastic and electromagnetic waves. Methods often utilized in both the literature and applications, such as the finite difference method [48], the finite element method [31, 37, 51] and the discontinuous Galerkin method [32, 50], rely on use of volumetric discretizations of the spatial domain in conjunction with appropriate time-stepping discretization methods. These volumetric discretization approaches can treat problems in general geometries and including spatially varying media. As is well known, however, these methods typically suffer from spatial and temporal numerical dispersion errors (also known as pollution errors [6, 38]), and they therefore require use of fine spatial and temporal meshes—and thus, large computer-memory and run-times—to achieve accurate solutions in applications involving high frequencies and/or long time simulations.

---

\*Department of Computing & Mathematical Sciences, California Institute of Technology, 1200 East California Blvd., CA 91125, United States. Email: [obruno@caltech.edu](mailto:obruno@caltech.edu)

†LSEC, Institute of Computational Mathematics and Scientific/Engineering Computing, Academy of Mathematics and Systems Science, Chinese Academy of Sciences, Beijing 100190, China. Email: [yintao@lsec.cc.ac.cn](mailto:yintao@lsec.cc.ac.cn)

The time-domain boundary integral equation method (TDBIE) for the wave equation, which, based on use of the retarded-potential Green’s function, only requires discretization of lower-dimensional domain boundary, has attracted attention recently [10, 13, 28, 44]. This method requires treatment of the Dirac delta function, and it therefore leads to integration domains given by the intersection of the light cone with the overall scattering surface. As a result, the schemes resulting from the discretization of the TDBIE are generally complex, and, additionally, they have presented challenges concerning numerical stability [10]. The “Convolution Quadrature” method [8, 13, 41, 45] (CQ), in turn, relies on the combination of a finite-difference time discretization and a Laplace-like transformation to reduce the time-domain problem to modified Helmholtz problems over a range of frequencies. The Helmholtz problems in the CQ context are tackled by means of frequency-domain integral equations, and, thus, the CQ method effectively eliminates spatial dispersion. The solution method inherits the dispersive character of the finite-difference approximation that underlies the time-domain scheme, however. A certain “infinite tail” in the CQ time history that results from “the passage through the Laplace domain” also presents “a serious disadvantage” [45, Chapter 5.1].

A frequency-time hybrid solver has recently been proposed [5], in which the time evolution is evaluated by means of a certain “windowing and time-recentering” procedure. The algorithm presented in that reference simply decomposes the incident time signal as a sum of a sequence of smooth compactly supported incident “wave packets”. Using Fourier transformation in time, the solution for each one of the wave packets is expressed in terms of regular-Helmholtz frequency-domain solutions—thus eliminating spatial dispersion, just like the CQ method. The “recentering” strategy then allows for use of a fixed set of frequency-domain solutions for arbitrarily long times. A tracking strategy is used to determine the time interval during which the solution associated with each wave packet must be kept as part of the simulation. An efficient implementation of the required Fourier transformation processes is introduced in [5] which includes specialized high-frequency algorithms, including, e.g. “time re-centering” of the wave as well as Chebyshev and Fourier Continuation Fourier-transform representations. Unlike other approaches, the hybrid method [5] has demonstrated time-domain solutions including complex scatterers, for incident fields applied over long periods of time. The method allows for time leaping, parallel-in-time implementation and, importantly, spectral accuracy in time. The CQ approach and other hybrid methods [27, 43], in contrast, have only provided solutions for incident signals of very brief time duration, as indicated in the various comparisons with other methods provided in [5].

The present paper proposes an extension of the time-domain method [5] to problems posed in interior physical domains. An immediate challenge arises as such a program is contemplated, namely, that the interior-domain Helmholtz equation is not uniquely solvable at any frequency whose negative square is an eigenvalue of the Laplace operator. This problem does not arise if the CQ method is used instead: the resulting modified Helmholtz problems are uniquely solvable for all Laplace frequencies. In order to avoid the aforementioned time-dispersion and infinite tail difficulties inherent in the CQ method, however, the present paper retains the use of the Fourier transform, and it re-expresses the full time-evolution as a problem of multiple scattering among various portions of the domain boundary. Thus, taking into account the wave’s finite speed of propagation, the original domain boundary is decomposed into a number  $N_{\text{arc}}$  of *overlapping* open-arcs, each one of which gives rise to a corresponding scattering problem, in absence of all other arcs in the decomposition; for simplicity, in this paper we restrict attention to the case  $N_{\text{arc}} = 2$ . In view of Theorem 2.7 below (see also Algorithms 1-4), by appropriately accounting for multiple scattering, solutions for such open-arc problems can be combined into a full solution, which is mathematically exact and numerically accurate, for the given interior domain problem. Crucially, the frequency-domain open-arc scattering problems that result upon Fourier transformation are uniquely solvable.

Solution via e.g. a Laplace transformation in time, in contrast, while also eliminating the difficulties arising from the existence of interior-eigenvalues (and associated lack of existence and uniqueness for the necessary frequency-domain problems), entails the instability inherent in numerical inverse Laplace

transformation. We suggest that this Laplace-transform instability reflects precisely the use of frequency-domain solutions that incorporate infinitely many multiple scattering events, from which the solution up to a given finite time  $T$  is then to be obtained—somehow eliminating, via high-frequency cancellations, all contributions from multiple scattering events beyond time  $T$ , and thereby, in view of such cancellations, incorporating a powerful source of ill conditioning at any finite spatio-temporal discretization level. Note that each frequency-domain solution in the Laplace frequency domain indeed contains infinite-time information, as is evidenced by the fact that the same set of frequency-domain solutions can theoretically be used to propagate the time-domain solution of the wave equation up to arbitrarily long times. The proposed multiple-scattering algorithm avoids the instability by restricting the number of multiple scattering events considered to what is strictly necessary to advance the solution up to a given finite time.

In the proposed algorithm the necessary frequency-domain open-arc scattering problems are obtained by means of a frequency-domain integral equation solver, as indicated in Algorithm 2. In view of the classical regularity theory for open-surface problems (see [26] and cf. [18, 39]), the open arc solutions are singular at the arc endpoints: they behave like a non-integer power of the distance to the endpoint and, e.g., in the case of Dirichlet boundary conditions considered in this paper, they tend to infinity as the endpoint is approached. The two-dimensional version [22] of the Chebyshev-based rectangular-polar discretization methodology [15], which incorporates a change of variables introduced in [21, Eq. (4.12)], is utilized to evaluate the corresponding integrals with a high order of accuracy. Together with an appropriate geometrical description, such as those provided by engineering NURBS-based models—which include parametrizations expressed in terms of certain types of Rational B-Splines—the overlapping-patch boundary-partitioning strategy can be used to tackle interior wave-equation problems in general three-dimensional engineering structures. Such extensions of the proposed methods, however, are not considered in this paper, and are left for future work.

This paper is organized as follows. Section 2.1 describes the wave propagation and scattering problem under consideration. Section 2.2 introduces the overlapping-arc scattering structure, and the time-domain boundary integral equations for the open-arc time-domain scattering problems. A necessary Huygens-like domain-of-influence condition is introduced in Section 2.3, which simply states that, as in free space, waves move along boundaries at the speed of sound. Surprisingly, to the best of the authors knowledge, such a result has not been established as yet. A discussion in this regard is presented in 2.3, including a rigorous proof of validity for the case of a circular boundary and clear numerical evidence of validity in other cases; the rigorous proof of validity of this condition for general curves is left for future work. As a byproduct of the constructions concerning the Huygens condition, a 2D double-layer time-domain formulation is introduced in Remark A.2 in Appendix A which bypasses certain difficulties encountered previously. On the basis of these materials, Section 2.4 re-expresses the interior time-domain problem in terms of a proposed open-arc “ping-pong” multiple-scattering approach, and it presents the main theoretical result of this paper, Theorem 2.7—which establishes that the interior time-domain problem is indeed equivalent to the proposed ping-pong problem. Section 2.5 then re-expresses the ping-pong problem in terms of associated open-arc frequency-domain problems, and Section 2.6 presents the windowing and time-recentering strategy that is used to enable the treatment of problems of arbitrary long time duration. The numerical implementation of the overall multiple scattering approach is presented in Section 3, including the windowed Fourier-transform algorithm [5] used (Section 3.1) and the frequency-domain layer-potentials employed (Section 3.2); the full computational implementation is outlined in Section 3.3. Numerical examples demonstrating the accuracy and efficiency of the proposed approach, finally, are presented in Section 4.

## 2 Hybrid frequency-time multiple scattering interior solver

### 2.1 Wave equation problem

Let  $\Omega \subset \mathbb{R}^2$  denote a bounded domain with piecewise smooth boundary  $\Gamma = \partial\Omega$ , and let  $u^i(x, t)$  denote a given smooth incident field defined for  $t \in \mathbb{R}$  and  $x \in \Gamma$ , which vanishes for  $t \leq 0$ . In what follows we consider the wave equation initial and boundary-value problem

$$\begin{cases} \frac{\partial^2 u^s}{\partial t^2}(x, t) - c^2 \Delta u^s(x, t) = 0, & (x, t) \in \Omega \times (-\infty, +\infty), \\ u^s(x, t) = 0, & (x, t) \in \Omega \times (-\infty, 0], \\ u^s(x, t) = -u^i(x, t), & (x, t) \in \Gamma \times (-\infty, +\infty) \end{cases} \quad (2.1)$$

for the scattered field  $u^s(x, t)$  throughout  $\Omega$ , where the constant  $c > 0$  denotes the wave-speed.

As indicated in Section 1, this paper proposes a fast hybrid method, related to that presented in [5], for the numerical solution of this problem. As noted in that section, however the frequency-domain solutions required by the hybrid method [5] fail to exist, in the present interior-domain context, at frequencies corresponding to Laplace eigenvalues in the domain  $\Omega$ —and, thus, the exterior-domain hybrid approach [5] does not apply in the present interior-domain context. The hybrid approach proposed in the present paper relies, instead, on a multiple scattering strategy that transforms the original wave equation problem in a bounded domain into a sequence of wave equation problems of scattering by overlapping *open-arcs*—for which the frequency domain solutions exist at all frequencies, and for which, therefore, general time-domain solutions can effectively be obtained via the windowing and recentering Fourier-transform methods introduced in [5]. The overlapping-arc scattering structure used as well as necessary theoretical results concerning open-arc time-domain scattering problems are presented in the following section.

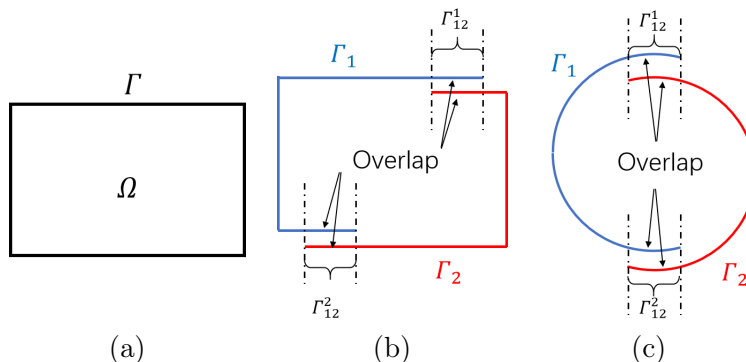


Figure 1: Decomposition of closed boundaries  $\Gamma$  into pairs of overlapping open arcs. (b) Decomposition of the rectangular boundary  $\Gamma$  depicted in (a); (c) Decomposition of a circular closed curve  $\Gamma$ .

### 2.2 Overlapping-arc geometry and time-domain boundary integral equations

The proposed multiple scattering algorithm relies on a boundary decomposition strategy based on use of overlapping patches. While the algorithm can utilize an arbitrary numbers of patches, for simplicity, this paper only considers decompositions consisting of two patches. Thus, as illustrated in Figure 1(b), the scattering surface  $\Gamma$  in Figure 1(a) is covered by two overlapping patches  $\Gamma_1 \subset \Gamma$  and  $\Gamma_2 \subset \Gamma$ ,  $\Gamma = \Gamma_1 \cup \Gamma_2$ , whose intersection  $\Gamma_{12} = \Gamma_1 \cap \Gamma_2$  equals the disjoint union  $\Gamma_{12} = \Gamma_{12}^1 \cup \Gamma_{12}^2$  of two connected components  $\Gamma_{12}^1$  and  $\Gamma_{12}^2$ . A similar decomposition is presented in Figure 1(c) for a different surface  $\Gamma$ . The “truncation” of  $\Gamma_1$  and  $\Gamma_2$  by  $\Gamma_{12}$  results in the truncated arcs  $\Gamma_j^{\text{tr}} = \Gamma_j \setminus \Gamma_{12}$ ,  $j = 1, 2$ . The distance between the arcs  $\Gamma_1^{\text{tr}}$  and  $\Gamma_2^{\text{tr}}$ , which is denoted by

$$\delta_{12} = \text{dist}\{\Gamma_1^{\text{tr}}, \Gamma_2^{\text{tr}}\}, \quad (2.2)$$

plays an essential role in our theory and algorithms.

Let us now consider the unbounded domains  $\Omega_j = \mathbb{R}^2 \setminus \Gamma_j$  ( $j = 1, 2$ ) and the corresponding time-domain problems of scattering by the arcs  $\Gamma_j$ , which play essential roles in the proposed multiple scattering algorithm. Given an incident signal  $g_j(x, t)$  defined for  $x \in \Gamma_j$  ( $j = 1, 2$ ) and  $t \in \mathbb{R}$ , which vanishes for  $t \leq 0$ , and using the trace operator  $\gamma_j : \Omega_j \rightarrow \Gamma_j$ , we consider the following wave equation problem for the function  $w_j^s(x, t)$ :

$$\frac{\partial^2 w_j^s}{\partial t^2}(x, t) - c^2 \Delta w_j^s(x, t) = 0, \quad (x, t) \in \Omega_j \times (-\infty, +\infty) \quad (2.3)$$

under the trivial conditions

$$w_j^s(x, t) = 0, \quad (x, t) \in \Omega_j \times (-\infty, 0], \quad (2.4)$$

and the Dirichlet boundary condition

$$w_j^s(x, t) = g_j(x, t), \quad (x, t) \in \Gamma_j \times (-\infty, +\infty). \quad (2.5)$$

As is well known [45], the solution  $w_j^s(x, t)$  admits the single-layer representation

$$w_j^s(x, t) = \tilde{\mathcal{S}}_j[\tilde{\psi}_j](x, t), \quad x \in \Omega_j, \quad (2.6)$$

where  $\tilde{\psi}_j$  is the solution of the time-domain integral equation

$$\tilde{\mathcal{S}}_j[\tilde{\psi}_j] = g_j \quad \text{on} \quad \Gamma_j. \quad (2.7)$$

Here the time-domain single-layer potential  $\tilde{\mathcal{S}}_j : H_\sigma^p(\mathbb{R}, \tilde{H}^{-1/2}(\Gamma_j)) \rightarrow H_\sigma^{p-1}(\mathbb{R}, H_{loc}^1(\Omega_j))$  is defined by

$$\tilde{\mathcal{S}}_j[\tilde{\psi}_j](x, t) = \frac{1}{2\pi} \int_{\Gamma_j} \int_0^{t-c^{-1}|x-y|} \frac{\tilde{\psi}_j(y, \tau)}{\sqrt{(t-\tau)^2 - c^{-2}|x-y|^2}} d\tau ds_y, \quad x \notin \Gamma_j, \quad (2.8)$$

and the time-domain single-layer boundary integral operator  $\tilde{\mathcal{S}}_j$  is given by

$$\tilde{\mathcal{S}}_j = \gamma \tilde{\mathcal{S}}_j : H_\sigma^p(\mathbb{R}, \tilde{H}^{-1/2}(\Gamma_j)) \rightarrow H_\sigma^{p-1}(\mathbb{R}, H^{1/2}(\Gamma_j)). \quad (2.9)$$

The space-time Sobolev space  $H_\sigma^p(\mathbb{R}, D)$  used above, where  $\sigma > 0$  and  $p \in \mathbb{R}$ , and where  $D$  denotes a Hilbert space, is defined by [7, 23]

$$H_\sigma^p(\mathbb{R}, D) := \left\{ f \in \mathcal{L}'_\sigma(D) : \int_{-\infty+i\sigma}^{\infty+i\sigma} |s|^{2p} \|\mathcal{L}[f](s)\|_D^2 ds < \infty \right\} \quad (2.10)$$

together with the norm

$$\|f\|_{H_\sigma^p(\mathbb{R}, D)} := \left( \int_{-\infty+i\sigma}^{\infty+i\sigma} |s|^{2p} \|\mathcal{L}[f](s)\|_D^2 ds \right)^{1/2}, \quad (2.11)$$

where  $\mathcal{L}[f]$  denotes the Fourier-Laplace transform of  $f$  given by

$$\mathcal{L}[f](s) := \int_{-\infty}^{\infty} f(t) e^{ist} dt, \quad s \in \mathbb{C}_\sigma := \{\omega \in \mathbb{C} : \text{Im}(s) > \sigma > 0\}, \quad (2.12)$$

and where  $\mathcal{L}'_\sigma(D) := \{\phi \in \mathcal{D}'_+(D) : e^{-\sigma t} \phi \in \mathcal{S}'_+(D)\}$  is defined in terms of the sets  $\mathcal{D}'_+(D)$  and  $\mathcal{S}'_+(D)$  of  $D$ -valued distributions and  $D$ -valued tempered distributions that vanish for  $t < 0$ , respectively. The wellposedness of the time-domain integral equation is given in the following theorem [23, 52].

**Theorem 2.1.** *The time-domain integral equation (2.7) admits a unique solution  $\tilde{\psi}_j \in H_\sigma^p(\mathbb{R}, \tilde{H}^{-1/2}(\Gamma_j))$ .*

### 2.3 Huygens-like domain-of-influence along boundaries

The multiple scattering algorithm proposed in this paper depends in an essential manner on a certain domain-of-influence condition, which we state as Condition 2.2 below, which is in essence a variant of the well known Huygens principle in a form that is applicable to the problem of scattering by obstacles and open arcs. Thus, Condition 2.2 expresses a well accepted principle in wave physics, namely, that solutions of the wave equation propagate at the speed of sound, and that the wave field vanishes identically before the arrival of a wavefront. This property has been rigorously established by the method of spherical means [9] for the problem of propagation of waves in space without scatterers. Further, some mathematical results have previously been given for the corresponding problem of scattering by obstacles [45, Proposition 3.6.2]. But previously available results for obstacle-scattering problems are not sharp, as they only ensure that the field propagates away from the complete boundary (with speed equal to the speed of sound), but they do not account for propagation *along* the scattering boundary. In particular, for incident fields illuminating a subset of the boundary of a scatterer, previous theoretical results do not establish that the field propagates at the speed of sound along the scattering boundary. Such a boundary-propagation result provides a crucial element in the proof of the main theorem of this paper, Theorem 2.7—which, showing that the exact solution of the problem (2.1) can be expressed as the sum of a series of multiple-scattering iterates, forms the basis of the ping-pong multiple-scattering algorithm proposed in this paper.

Although we conjecture that Condition 2.2 is always valid, to the best of our knowledge such a result has not previously been established. Whereas a treatment of this problem is beyond the scope of this paper, in Lemma 2.3 we do present a proof for the case in which  $\Gamma$  is a circular arc. Additionally, we have numerically verified the validity of this condition for a wide range of arcs; one such example is presented in Section 2.3.1 below.

For the sake of brevity we present the necessary Huygens-like condition in exactly the form that will be needed in the proof of Theorem 2.7, but, clearly, alternative expressions of the same concept, not involving the specifics of the proof of the theorem, can easily be put forth. In particular, to match the setting of the theorem, for an integer  $j$  we introduce the notation

$$j' = \text{mod}(j, 2) + 1 \quad (j \in \mathbb{N}), \quad (2.13)$$

where, for integers  $a$  and  $b$ ,  $\text{mod}(a, b)$  denotes the remainder of the division of  $a$  by  $b$ . In our context, where the index values  $j = 1, 2$  refer to the corresponding arcs  $\Gamma_1, \Gamma_2$ , we have  $j' = 1$  (resp.  $j' = 2$ ) for  $j = 2$  (resp.  $j = 1$ ). Using this notation, the necessary Huygens-like condition is stated in what follows.

**Condition 2.2.** *Let  $j \in \{1, 2\}$  and  $T_0 > 0$ , and assume*

$$g_j(x, t) = 0 \quad \text{for } (x, t) \in \Gamma_j \times (-\infty, T_0] \cup \Gamma_{12} \times (-\infty, +\infty). \quad (2.14)$$

*Then, recalling equation (2.2), letting  $t_0 = \delta_{12}/c > 0$ , and calling  $w_j^s$  the solution of the wave equation problem (2.3)-(2.5), we have*

$$w_j^s(x, t) = 0 \quad \text{for } (x, t) \in \Gamma_{j'}^{\text{tr}} \times (-\infty, T_0 + t_0). \quad (2.15)$$

The validity of Condition 2.2 for the case that  $\Gamma$  is a circle is established in the following lemma; as indicated above, the proof for general curves  $\Gamma$  is left for future work.

**Lemma 2.3.** *Let  $R > 0$  and  $\Gamma = \{x \in \mathbb{R}^2 \mid |x| = R\}$ . Then Condition 2.2 holds for the decomposition  $\Gamma = \Gamma_1 \cup \Gamma_2$  of the type depicted in Figure 1(c).*

Before proceeding with the proof of Lemma 2.3 we establish, in Lemma 2.4, a certain Huygens-like condition for the solution  $v^s(x, t)$  of the wave equation problem

$$\begin{cases} \frac{\partial^2 v^s}{\partial t^2}(x, t) - c^2 \Delta v^s(x, t) = 0, & (x, t) \in (\mathbb{R}^2 \setminus \Gamma) \times \mathbb{R}, \\ v^s(x, t) = 0, & (x, t) \in (\mathbb{R}^2 \setminus \Gamma) \times (-\infty, 0], \\ v^s(x, t) = f(x, t), & (x, t) \in \Gamma \times \mathbb{R}, \end{cases} \quad (2.16)$$

inside/outside the ball  $B_R := \{x \in \mathbb{R}^2 \mid |x| < R\}$  of radius  $R$ .

**Lemma 2.4.** *Let  $\Gamma^{\text{inc}} \subset \Gamma$  be given and assume that, (a)  $f$  vanishes for  $t \leq 0$ , and, (b)  $f$  satisfies*

$$\{x \in \Gamma \mid f(x, t) \neq 0\} \subset \Gamma^{\text{inc}} \quad \text{for all } t > 0. \quad (2.17)$$

We then have

$$\{x \in \mathbb{R}^2 \mid v^s(x, t) \neq 0\} \subset \Lambda^s(t) \quad \text{for all } t > 0, \quad (2.18)$$

where

$$\Lambda^s(t) = \{x \in \mathbb{R}^2 \mid \text{dist}(x, \Gamma^{\text{inc}}) \leq ct\}.$$

*Proof.* To establish (2.18) we utilize the Green's function  $G_\omega(x, y)$  for the circle  $\Gamma$ , which, for each  $y \in \mathbb{R}^2 \setminus \overline{B_R}$  is defined as the solution of the problem

$$\begin{cases} \Delta_x G_\omega(x, y) + \kappa^2 G_\omega(x, y) = -\delta_y(x), & (x, \omega) \in \mathbb{R}^2 \setminus \overline{B_R} \times \mathbb{R}, \quad \kappa = \omega/c, \\ G_\omega(x, y) = 0 & (x, \omega) \in \Gamma \times \mathbb{R}. \end{cases}$$

As is well known, the method of images yields

$$G_\omega(x, y) = \frac{i}{4} H_0^{(1)}(\kappa|x-y|) - \frac{i}{4} H_0^{(1)}(\kappa R^{-1}|x||x'-y|), \quad x \neq y, \quad (2.19)$$

where  $x' = xR^2|x|^{-2} \in B_R$  denotes the image point of  $x \in \mathbb{R}^2 \setminus \overline{B_R}$  with respect to  $\Gamma$ , and where  $H_0^{(1)}$  denotes the Hankel function of first kind and order zero. Let now  $V^s(x, \omega)$  denote the Fourier transform of  $v^s(x, t)$  with respect to  $t$  for  $x \in \mathbb{R}^2 \setminus \overline{B_R}$ ; clearly  $V^s$  is a solution of the Helmholtz equation with wavenumber  $\kappa$  outside  $B_R$ , and with Dirichlet boundary conditions  $V^s = F$  on  $\Gamma$ —where  $F(x, \omega)$  denotes the Fourier transform of  $f(x, t)$  with respect to  $t$ . Use of Green's theorem together with the Green function  $G_\omega$  yields

$$V^s(x, \omega) = \int_\Gamma \partial_{\nu_y} G_\omega(x, y) F(y, \omega) ds_y, \quad x \in \mathbb{R}^2 \setminus \overline{B_R}. \quad (2.20)$$

In view of equation (A.5) in the Appendix A, it follows that

$$v^s(x, t) = \frac{1}{2\pi c^2 R} \int_{\Gamma^{\text{inc}}} \int_0^{t-c^{-1}|x-y|} \left[ \frac{|x-y|(|x|^2 - R^2)f(y, \tau)}{(t-\tau)^2 \sqrt{(t-\tau)^2 - c^{-2}|x-y|^2}} + \frac{|x-y|(|x|^2 - R^2)f^{(1)}(y, \tau)}{(t-\tau) \sqrt{(t-\tau)^2 - c^{-2}|x-y|^2}} \right] d\tau ds_y \quad (2.21)$$

for all  $x \in \mathbb{R}^2 \setminus \overline{B_R}$  and all  $t > 0$ . Noting that for  $t > 0$  and  $x \notin \Lambda^s(t)$  we have  $t - c^{-1}|x-y| < 0$  for all  $y \in \Gamma^{\text{inc}}$ , and since  $f(\cdot, t) = 0$  for all  $t \leq 0$  by assumption, (2.18) follows for the solution outside  $B_R$ . The result for the solution inside  $B_R$  can be proved in a similar manner and the proof is complete.  $\square$

Using Lemma 2.4, the proof of Lemma 2.3 follows easily.

*Proof of Lemma 2.3.* Call  $\Gamma^{\text{inc}} = \Gamma_j^{\text{tr}}$  ( $j = 1$  or  $j = 2$ ), let  $f = g_j$  on  $\Gamma^{\text{inc}}$  and  $f = 0$  on  $\Gamma \setminus \Gamma^{\text{inc}}$ . Then, in view of (2.18), for all  $x \notin \Gamma$  the solution  $v^s(x, t)$  of the wave-equation problem (2.16) satisfies

$$\gamma_D^- v^s(x, t) = \gamma_D^+ v^s(x, t) = 0 \quad \text{and} \quad \gamma_N^- v^s(x, t) = \gamma_N^+ v^s(x, t) = 0 \quad \text{for } x \in \Gamma_j^{\text{tr}} \quad \text{and } t \leq t_0,$$

where  $\gamma_D^\pm, \gamma_N^\pm$  denote the (interior (-), exterior (+)) Dirichlet and Neumann traces, respectively. It follows that  $v^s(x, t)$  satisfies the open-arc boundary condition (2.5) and is smooth across the boundary  $\Gamma_j^{\text{tr}}$  for  $t < t_0$ , which shows that  $v^s(x, t) = w_j^s(x, t)$  for  $x \in \mathbb{R}^2 \setminus \Gamma_j$  and  $t < t_0$  and, thus, Condition 2.2 follows immediately from (2.18).

### 2.3.1 Numerical verification of Condition 2.2 for open and closed elliptical boundaries.

As indicated above, we have conducted a number of numerical tests that clearly suggest, as expected, Condition 2.2 is universally valid. For reference we present one such test case in this section. To introduce our example we let

$$\begin{aligned}\Gamma_1 &= \{x = (\cos \theta, 1.5 \sin \theta) : \theta \in (0.5\pi, 1.5\pi)\}, \\ \Gamma_2^{\text{tr}} &= \{x = (\cos \theta, 1.5 \sin \theta) : \theta \in (-0.5\pi, 0.5\pi)\}, \\ \Gamma_{12} &= \{x = (\cos \theta, 1.5 \sin \theta) : \theta \in (0.5\pi, 0.75\pi) \cup (1.25\pi, 1.5\pi)\},\end{aligned}$$

and we consider the wave equation problem (2.3)-(2.5) with  $j = 1$  and

$$g_1(x, t) = \begin{cases} [1 - \cos 4(\theta - 0.75\pi)] \exp(-16(t - 3)^2), & (x, t) = (\cos \theta, 1.5 \sin \theta) \in \Gamma_1^{\text{tr}} \times (T_0, \infty), \\ 0, & (x, t) \in \Gamma_{12} \times (T_0, \infty), \\ 0, & (x, t) \in \Gamma_1 \times (-\infty, T_0]. \end{cases}$$

where  $T_0 = 1.74$ . (This selection of  $T_0$  makes  $g_1(x, t)$  “approximately continuous” at  $t = T_0$ , since, as is easily checked,  $[1 - \cos 4(\theta - 0.75\pi)] \exp(-16(t - 3)^2) < 10^{-11}$  for  $(x, t) \in \Gamma_1^{\text{tr}} \times (-\infty, T_0)$ .) It can also be checked that  $t_0 = \delta_{12}/c \approx 0.83$  for the geometry under consideration.

Table 1 presents the maximum values of  $|w_1^s(x, t)|$  in different time intervals at four points on  $\Gamma_2^{\text{tr}}$

$$x_1 = (0.031, 1.499), \quad x_2 = (0.5, 1.299), \quad x_3 = (0.866, 0.75), \quad x_4 = (1, 0);$$

note, in particular, that the point  $(0.031, 1.499)$  is very close to  $\Gamma_1$ . The first column in this table shows that for all four points  $x \in \Gamma_2^{\text{tr}}$  and for  $t < T_0 + t_0$ , the relation (2.15) is verified up to the numerical accuracy of the solution. Further, letting  $t_\ell = c^{-1} \text{dist}\{x_\ell, \Gamma_1^{\text{tr}}\}$ ,  $\ell = 2, 3, 4$  which gives

$$t_2 \approx 1.23, \quad t_3 \approx 1.60 \quad \text{and} \quad t_4 = 2.$$

The maximum values of  $|w_1^s(x_\ell, t)|$  listed in the second, third and fourth columns in Table 1, which correspond to the time intervals  $t \in (0, T_0 + t_0 + t_\ell)$ ,  $\ell = 2, 3, 4$ , illustrate, more generally, the Huygens-like domain-of-influence property

$$w_1^s(x, t) = 0 \quad \text{for} \quad (x, t) \in \Gamma_2^{\text{tr}} \times (-\infty, T_0 + t_x), \quad t_x = c^{-1} \text{dist}\{x, \Gamma_1^{\text{tr}}\}.$$

Table 1: Maximum values of  $|w_1^s(x, t)|$  in different time intervals at different points on  $\Gamma_2^{\text{tr}}$ .

$x$	$\max_{t \in (0, T_0 + t_0)}  w_1^s(x, t) $	$\max_{t \in (0, T_0 + t_0 + t_2)}  w_1^s(x, t) $	$\max_{t \in (0, T_0 + t_0 + t_3)}  w_1^s(x, t) $	$\max_{t \in (0, T_0 + t_0 + t_4)}  w_1^s(x, t) $
$x_1$	$1.81 \times 10^{-12}$	$2.32 \times 10^{-8}$	$1.71 \times 10^{-4}$	$1.70 \times 10^{-2}$
$x_2$	$4.59 \times 10^{-12}$	$4.59 \times 10^{-12}$	$1.29 \times 10^{-7}$	$1.49 \times 10^{-3}$
$x_3$	$5.23 \times 10^{-12}$	$5.23 \times 10^{-12}$	$5.23 \times 10^{-12}$	$7.93 \times 10^{-7}$
$x_4$	$6.98 \times 10^{-12}$	$7.17 \times 10^{-12}$	$7.39 \times 10^{-12}$	$2.61 \times 10^{-11}$

## 2.4 Two-arc “ping-pong” multiple scattering construction

Taking into account the finite propagation speed that characterizes the solutions of the wave equation, we propose to produce the time-domain solution of the original problem (2.1) in the interior domain  $\Omega$  as the sum of “ping-pong” wave-equation solutions multiply scattered by the arcs  $\Gamma_1$  and  $\Gamma_2$ . To describe the ping-pong multiple-scattering scheme we introduce a few useful notations and conventions. We call

$$j(m) = 2 - \text{mod}(m, 2), \quad m = 1, 2, 3, \dots \quad (2.22)$$



(in other words,  $j(m)$  equals 1 or 2 depending on whether  $m$  is odd or even, respectively), and, as detailed in Definition 2.5, we inductively define boundary-condition functions  $f_m(x, t)$  ( $m \geq 1$ ) and associated wave-equation solutions  $v_m(x, t)$  ( $m \geq 1$ ), all of which are *causal*—that is to say, they vanish identically for  $t \leq 0$ .

**Definition 2.5.** For  $m \in \mathbb{N}$  we inductively define  $v_m^s(x, t)$  as equal to the solution  $w_{j(m)}^s(x, t)$  of the open-arc problem (2.3)–(2.5) with boundary data

$$v_m^s(x, t) = f_m(x, t) \quad \text{for } (x, t) \in \Gamma_{j(m)} \times (-\infty, \infty), \quad (m \in \mathbb{N}), \quad (2.23)$$

where  $f_m(x, t) : \Gamma_{j(m)} \times (-\infty, \infty) \rightarrow \mathbb{C}$  denotes the causal functions defined inductively via the relations

$$f_1(x, t) = -u^i(x, t) \quad \text{on } \Gamma_1, \quad f_2(x, t) = -u^i(x, t) - v_1^s(x, t) \quad \text{on } \Gamma_2, \quad (2.24)$$

and,

$$f_m(x, t) = -v_{m-1}^s(x, t), \quad \text{on } \Gamma_{j(m)}, \quad m \geq 3. \quad (2.25)$$

**Remark 2.6.** The proposed multiple-scattering strategy relies crucially on the relations

$$f_m(x, t) = 0 \quad \text{for } (x, t) \in \Gamma_{12} \times (-\infty, \infty), \quad m \in \mathbb{N}, \quad m \geq 2, \quad (2.26)$$

which can easily be established inductively, as indicated in what follows. Considering first the case  $m = 2$ , in view of Definition 2.5, we have  $v_2^s(x, t) = f_2(x, t) = -u^i(x, t) - v_1^s(x, t)$  on  $\Gamma_2$ , on one hand, and  $v_1^s(x, t) = -u^i(x, t)$  on  $\Gamma_1$ , on the other. We conclude that  $v_2^s(x, t) = 0$  for  $(x, t) \in \Gamma_{12} \times (-\infty, \infty)$ , as desired. The inductive step is equally simple: assuming, for  $\ell \in \mathbb{N}, \ell \geq 2$ , that  $f_\ell(x, t)$  vanishes for  $(x, t) \in \Gamma_{12} \times (-\infty, \infty)$ , and in view of (2.23) and (2.25), we have  $f_{\ell+1}(x, t) = -v_\ell^s(x, t) = -f_\ell(x, t) = 0$  for  $(x, t) \in \Gamma_{12} \times (-\infty, \infty)$ , and (2.26) follows.

The main theorem of this paper, which is presented in what follows, concerns an  $M$ -th order multiple-scattering sum

$$u_M^s(x, t) := \sum_{m=1}^M v_m^s(x, t), \quad (2.27)$$

which includes contributions from all  $M$  “ping-pong” scattering iterates  $v_m^s(x, t)$  with  $m = 1, \dots, M$ .

**Theorem 2.7.** Let  $M \in \mathbb{N}, M \geq 2$ , and denote  $T = T(M) = (M - 1)\delta_{12}/c$ . Further, assume that Condition 2.2 holds. Then, for all  $(x, t) \in \Omega \times [-\infty, T(M)]$  we have  $u^s(x, t) = u_M^s(x, t)$ .

*Proof.* By construction,  $u_M^s(x, t)$  is a continuous function in  $\bar{\Omega} \times (-\infty, \infty)$  which satisfies the homogeneous wave equation and the trivial condition for  $(x, t) \in \Omega \times (-\infty, 0]$ . Thus, by uniqueness of solution of the problem (2.1) [30], to complete the proof of the theorem it suffices to show that for all  $M \in \mathbb{N}, M \geq 2$ , the function  $u_M^s$  satisfies

$$u_M^s(x, t) + u^i(x, t) = 0 \quad \text{for } (x, t) \in \Gamma \times (-\infty, T(M)]. \quad (2.28)$$

The validity of the relation (2.28), and thus, the proof of the theorem, are established in what follows by induction on the integer  $M$ .

We thus first seek to verify the relation (2.28) in the case  $M = 2$ . Since  $u_2^s(x, t) = v_1^s(x, t) + v_2^s(x, t)$  for  $(x, t) \in \Gamma \times (-\infty, \infty)$ , to establish the  $M = 2$  result it suffices to show that

$$v_1^s(x, t) + v_2^s(x, t) + u^i(x, t) = 0 \quad \text{for } (x, t) \in \Gamma \times (-\infty, \delta_{12}/c], \quad (2.29)$$

which, in view of (2.24), results from the conditions

$$v_1^s(x, t) + v_2^s(x, t) + u^i(x, t) = 0 \quad \text{for } (x, t) \in \Gamma_2 \times (-\infty, \infty) \quad (2.30)$$

and

$$v_2^s(x, t) = 0 \quad \text{for } (x, t) \in \Gamma_1^{\text{tr}} \times (-\infty, \delta_{12}/c]. \quad (2.31)$$

Equation (2.30) follows immediately from Definition 2.5 since per (2.23) and (2.24) we have  $v_2^s(x, t) = f_2(x, t) = -u^i(x, t) - v_1^s(x, t)$  on  $\Gamma_2$  for all  $t \in \mathbb{R}$ . To verify (2.31), we note from (2.26) that  $f_2(x, t)$  vanishes for  $(x, t) \in \Gamma_{12} \times (-\infty, \infty)$ . Then in view of Condition 2.2, equation (2.31) results and thus, the proof for the case  $M = 2$  follows.

Using the notation  $j'(m) = \text{mod}(j(m), 2) + 1$  (equation (2.13)), to complete the inductive proof we assume that for any  $M \in \mathbb{N}$  with  $2 \leq M \leq L$ ,  $L \geq 2$ , the following two relations hold:

$$u_M^s(x, t) + u^i(x, t) = 0 \quad \text{for } (x, t) \in \Gamma_{j(M)} \times (-\infty, \infty), \quad (2.32)$$

and

$$v_M^s(x, t) = 0 \quad \text{for } (x, t) \in \Gamma_{j'(M)}^{\text{tr}} \times (-\infty, (M-1)\delta_{12}/c]. \quad (2.33)$$

We then show that the same relations and, as a result, the relation (2.28), hold for  $M = L + 1$ . To do this we note that equation (2.25) tells us that  $v_{L+1}^s(x, t) + v_L^s(x, t) = 0$  for  $(x, t) \in \Gamma_{j(L+1)} \times (-\infty, \infty)$ . Therefore, the  $M = L - 1$  condition (2.32) implies that

$$u_{L+1}^s(x, t) + u^i(x, t) = v_{L+1}^s(x, t) + v_L^s(x, t) + u_{L-1}^s(x, t) + u^i(x, t) = 0 \quad (2.34)$$

for  $(x, t) \in \Gamma_{j(L+1)} \times (-\infty, \infty)$ . Noting that  $j'(L) = j(L + 1)$  and using (2.26) and (2.33) with  $M = L$  we see that  $f_{L+1}(x, t) = 0$  for  $(x, t) \in \Gamma_{j(L+1)} \times (-\infty, (L-1)\delta_{12}/c] \cup \Gamma_{12} \times (-\infty, +\infty)$ , and, thus, Condition 2.2 tells us that

$$v_{L+1}^s(x, t) = 0 \quad \text{for } (x, t) \in \Gamma_{j'(L+1)}^{\text{tr}} \times (-\infty, L\delta_{12}/c], \quad (2.35)$$

or, in other words, the relations (2.32) and (2.33) hold for  $M = L + 1$ . Combining the relation (2.33) and the condition (2.32) for  $M = L$ , it follows that

$$u_{L+1}^s(x, t) + u^i(x, t) = v_{L+1}^s(x, t) + u_L^s(x, t) + u^i(x, t) = 0 \quad (2.36)$$

for  $(x, t) \in \Gamma_{j'(L+1)}^{\text{tr}} \times (-\infty, L\delta_{12}/c]$ . The relation (2.28) for  $M = L + 1$  results from (2.34) and (2.36), which completes the proof.  $\square$

The proposed multiple scattering strategy for the solution of the wave equation problem (2.1) for  $(x, t) \in \Omega \times (-\infty, T(M)]$  ( $M = 2, 3, \dots$ ), which is embodied in Theorem 2.7, the associated ping-pong solutions  $v_m^s$ , and the sum (2.27) ( $m = 1, \dots, M$ ), is summarized in Algorithm 1. Note that, in this algorithm, the necessary solutions  $v_m^s(x, t)$  are obtained by means of the hybrid frequency-time approach presented in Section 2.5.

---

**Algorithm 1** Multiple scattering algorithm

---

- 1: Do  $m = 1, 2, \dots, M$
  - 2:   Evaluate the boundary data  $f_m$  via relations (2.24)-(2.25).
  - 3:   Compute  $v_m^s(x, t)$ ,  $(x, t) \in (\Omega \cup \Gamma_{j'(m)}) \times (-\infty, T(M)]$  using the open-arc hybrid solver presented in Section 2.5.
  - 4: End Do
  - 5: Compute  $u_M^s(x, t)$ ,  $(x, t) \in \Omega \times (-\infty, T(M)]$  using equation (2.27).
-

## 2.5 Frequency-domain multiple scattering algorithm

Call  $F(\omega)$  denote the Fourier transform of a function  $f(t) \in L^2(\mathbb{R})$ ,

$$F(\omega) = \mathbb{F}(f)(\omega) := \int_{-\infty}^{+\infty} f(t)e^{i\omega t} dt, \quad (2.37)$$

and let the corresponding inverse Fourier transform of a frequency-domain function  $F \in L^2(\mathbb{R})$  be denoted by

$$f(t) = \mathbb{F}^{-1}(F)(\omega) := \frac{1}{2\pi} \int_{-\infty}^{+\infty} F(\omega)e^{-i\omega t} d\omega. \quad (2.38)$$

Then, letting  $\kappa = \omega/c$  denote the spatial wave number, the Fourier transform  $V_m^s(x, \omega)$  of the solution  $v_m^s(x, t)$  of the wave equation is a solution of the Helmholtz equation  $\Delta V_m^s + \kappa^2 V_m^s = 0$  in  $\Omega_{j(m)}$  with Dirichlet boundary conditions  $V_m^s = F_m$  on  $\Gamma_{j(m)}$  where  $F_m(x, \omega) = \mathbb{F}(f_m)(x, \omega)$ . As is well known, the solution  $V_m^s(x, \omega)$  admits the representation

$$V_m^s(x, \omega) = \mathcal{S}_{j(m)}[\psi_m](x, \omega) := \int_{\Gamma_{j(m)}} \Phi_\omega(x, y)\psi_m(y)ds_y, \quad x \in \Omega_{j(m)}, \quad (2.39)$$

where  $\psi_m$  is the solution of the integral equation

$$\mathcal{S}_{j(m)}[\psi_m] = F_m \quad \text{on} \quad \Gamma_{j(m)}. \quad (2.40)$$

Here  $S_j : \tilde{H}^{-1/2}(\Gamma_j) \rightarrow H^{1/2}(\Gamma_j)$  denotes the single-layer operator

$$S_j[\psi](x, \omega) := \int_{\Gamma_j} \Phi_\omega(x, y)\psi(y)ds_y, \quad x \in \Gamma_j, \quad (2.41)$$

where  $H_0^{(1)}$  denotes the Hankel function of first kind, and where  $\Phi_\omega(x, y) = \frac{i}{4}H_0^{(1)}(\kappa|x-y|)$  denotes the fundamental solution of the Helmholtz equation  $\Delta w + \kappa^2 w = 0$  in  $\mathbb{R}^2$ . Our approach relies on the existence and uniqueness of solution of equation (2.40), which are guaranteed by the following theorem.

**Theorem 2.8.** *Given  $F_m \in H^{1/2}(\Gamma_{j(m)})$  the integral equation (2.40) admits a unique solution in  $\tilde{H}^{-1/2}(\Gamma_j)$  for any frequency  $\omega > 0$ .*

*Proof.* Provided in [46]. □

In view of Definition 2.5, the boundary function  $F_m$  is determined inductively by the relations

$$F_1(x, \omega) = -\mathbb{F}(u^i)(x, \omega) \quad \text{on} \quad \Gamma_1, \quad F_2(x, \omega) = -\mathbb{F}(u^i)(x, \omega) - V_{1,m-1}^s(x, \omega) \quad \text{on} \quad \Gamma_2, \quad (2.42)$$

and,

$$F_m(x, \omega) = -V_{m-1}^s(x, \omega) \quad \text{on} \quad \Gamma_{j(m)}, \quad m \geq 3. \quad (2.43)$$

The frequency-domain component of the proposed frequency-time hybrid multiple scattering algorithm, which produces the solutions  $v_m^s$  for  $m = 1, \dots, M$ , is obtained by re-expressing Algorithm 1 via an application of the Fourier transform. The result is Algorithm 2 below.

---

### Algorithm 2 Hybrid multiple scattering algorithm

---

- 1: Do  $m = 1, 2, \dots, M$
  - 2: Evaluate the boundary data  $F_m$  via relations (2.42)-(2.43).
  - 3: Solve the integral equation (2.40) with solution  $\psi_m$ .
  - 4: Compute  $V_m^s(x, \omega)$ ,  $(x, \omega) \in (\Omega \cup \Gamma_{j'(m)}) \times (-\infty, +\infty)$  via (2.39).
  - 5: Compute  $v_m^s(x, t) = \mathbb{F}^{-1}(V_m^s)(x, t)$ ,  $(x, t) \in (\Omega \cup \Gamma_{j'(m)}) \times [0, T(M)]$ .
  - 6: End Do
-

## 2.6 Windowing and time-recentering

For a given signal  $f_m(x, t)$ , the time-domain open-arc solution described in Section 2.5 is obtained via the following sequence of operations:

$$f_m(x, t) \xrightarrow{\mathbb{F}} F_m(x, \omega) \xrightarrow{(2.39), (2.40)} V_m^s(x, \omega) \xrightarrow{\mathbb{F}^{-1}} v_m^s(x, t). \quad (2.44)$$

Clearly, the function  $f_m(x, t)$  may represent a signal of arbitrarily long duration: this is merely a smooth compactly supported function for  $t \in [0, T]$ , with a potentially large value of  $T > 0$ . For such large values of  $T$  the Fourier transform  $F_m(x, \omega)$  is generally a highly oscillatory function of  $\omega$ , as a result of the fast oscillations in the Fourier transform integrand factor  $e^{i\omega t}$ —see e.g. [5, Fig. 1]. Under such a scenario a very fine frequency-discretization, requiring  $\mathcal{O}(T)$  frequency points, and, thus, a number  $\mathcal{O}(T)$  of evaluations of the frequency-domain boundary integral equation solver, is required to obtain the time-domain solution  $v_m^s(x, t)$ . This makes the overall algorithm unacceptably expensive for long-time simulations. To overcome these difficulties, a certain “windowing and time-recentering” procedure was proposed in [5, Sec. 3.1], that decomposes a scattering problem involving an incident time signal of long duration into a sequence of problems with smooth incident field of a limited duration, all of which can be solved in terms of a fixed set of solutions of the corresponding frequency-domain problems for arbitrarily large values of  $T$ .

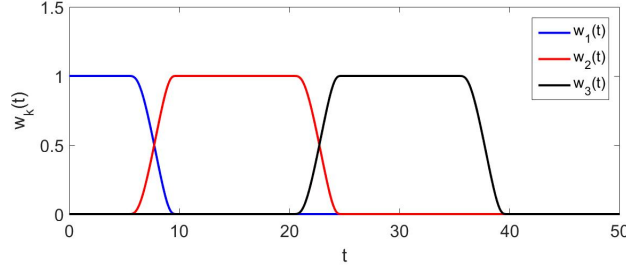


Figure 2: Windowing functions  $w_k(t)$ ,  $k = 1, 2, 3$  with  $H = 10$ .

For a given final time  $T$ , the windowing-and-recentering approach is based on use of a smooth partition of unity  $\mathcal{P} = \{\chi_k(t) \mid k \in \mathcal{K}\}$ ,  $\mathcal{K} = \{1, \dots, K\}$ , where the functions  $\chi_k$  satisfy  $\sum_{k \in \mathcal{K}} \chi_k(t) = 1$  for  $t \in [0, T]$  and, for a certain sequence  $s_k$  ( $k \in \mathcal{K}$ ), each  $\chi_k(t)$  is a non-negative, smooth windowing function of  $t$ , supported in the interval  $[s_k - H, s_k + H]$  of duration  $2H$ . The partition-of-unity  $\mathcal{P}$  can be generated on the basis of the smooth function  $\eta(t; t_0, t_1)$  given by

$$\eta(t; t_0, t_1) = \begin{cases} 1, & |t| \leq t_0, \\ e^{\frac{2e^{-1/s}}{s-1}}, & t_0 < |t| < t_1, s = \frac{|t|-t_0}{t_1-t_0}, \\ 0, & |t| \geq t_1. \end{cases} \quad (2.45)$$

Without loss of generality, in this work we set

$$H = \frac{T}{3K/2 - 1}, \quad s_k = \frac{3}{2}(k-1)H, \quad (2.46)$$

and

$$\chi_k(t) = \chi(t - s_k), \quad \chi(s) = \begin{cases} \eta(s/H; 1/2, 1), & -H/2 \leq s \leq H, \\ 1 - \eta(s/H + 3/2; 1/2, 1), & -H < s < -H/2; \\ 0, & |s| \geq H; \end{cases}$$

—a prescription that clearly ensures that  $s_K + H/2 = T$  and  $\sum_{k=1}^K \chi_k(t) = 1$  for all  $t \in [0, T]$ . A depiction of such a partition of unity, with  $H = 10$ , is presented in Figure 2.

Utilizing the partition-of-unity  $\mathcal{P}$ , any smooth long-time signal  $f(t)$ ,  $t \in [0, T]$ , can be expressed in the form

$$f(t) = \sum_{k \in \mathcal{K}} f_k(t), \quad f_k(t) = f(t)\chi_k(t), \quad (2.47)$$

where  $f_k$  is compactly supported in  $[s_k - H, s_k + H]$ . The corresponding Fourier transform is then given by

$$F(\omega) = \sum_{k \in \mathcal{K}} F_k(\omega), \quad F_k(\omega) = \int_0^{T_0} f_k(t)e^{i\omega t} dt = e^{i\omega s_k} F_{k,slow}(\omega), \quad (2.48)$$

where, defining by

$$\mathbb{F}_{k,slow}(f)(\omega) := \int_{-H}^H f(t + s_k)\chi_k(t)e^{i\omega t} dt,$$

the  $s_k$ -centered slow Fourier-transform operator, we call  $F_{k,slow}(\omega) = \mathbb{F}_{k,slow}(f)(\omega)$ ; note that, as suggested by the notation used,  $F_{k,slow}$  is a slowly-oscillatory function of  $\omega$ .

For  $k \in \mathcal{K}$ , we now call  $F_{m,k} = \mathbb{F}_{k,slow}(f_m)$  the slow Fourier-transform of the  $m$ -th iterate  $f_m$ , and we let

$$V_{m,k}^s(x, \omega) = \mathcal{S}_{j(m)}[\psi_{m,k}](x, \omega), \quad (2.49)$$

where  $\psi_{m,k}$  is the solution of the integral equation

$$\mathcal{S}_{j(m)}[\psi_{m,k}] = F_{m,k} \quad \text{on} \quad \Gamma_{j(m)}. \quad (2.50)$$

It follows that

$$F_m(x, \omega) = \sum_{k \in \mathcal{K}} e^{i\omega s_k} F_{m,k}(x, \omega), \quad (2.51)$$

and

$$v_m^s(x, t) = \sum_{k \in \mathcal{K}} \mathbb{F}^{-1}(V_{m,k}^s)(x, t - s_k); \quad (2.52)$$

note that  $\mathbb{F}^{-1}(V_{m,k}^s)(x, t) = 0$  for  $t < s_k - H$ . Adopting the time-recentering strategy described in this section, Algorithm 2 leads to the more efficient Algorithm 3.

---

**Algorithm 3** Hybrid multiple scattering algorithm with time-recentering

---

- 1: Do  $m = 1, 2, \dots, M$
  - 2: Evaluate the boundary data  $f_m(x, t)$ ,  $(x, t) \in \Gamma_{j(m)} \times [0, s_K + H]$  via relations (2.24)-(2.25).
  - 3: Set  $v_m^s(x, t) = 0$ ,  $(x, t) \in (\Omega \times [0, T]) \cup (\Gamma_{j'(m)} \times [0, s_K + H])$ .
  - 4: Do  $k = 1, 2, \dots, K$
  - 5: Evaluate the boundary data  $F_{m,k}(x, \omega) = \mathbb{F}_{k,slow}(f_m)(x, \omega)$ ,  $(x, \omega) \in \Gamma_{j(m)} \times (-\infty, \infty)$ .
  - 6: Solve the integral equation (2.50) with solution  $\psi_{m,k}$ .
  - 7: Compute  $V_{m,k}^s(x, \omega)$ ,  $(x, \omega) \in (\Omega \cup \Gamma_{j'(m)}) \times (-\infty, \infty)$  through (2.49).
  - 8: Compute  $v_m^s(x, t) += \mathbb{F}^{-1}(V_{m,k}^s)(x, t - s_k)$ ,  $(x, t) \in (\Omega \times [0, T]) \cup (\Gamma_{j'(m)} \times [0, s_K + H])$ .
  - 9: End Do
  - 10: End Do
-

### 3 Hybrid multiple scattering strategy: numerical implementation

This section presents algorithms necessary for the numerical implementation of the hybrid multiple scattering strategy introduced in Algorithm 3, including algorithms for accurate evaluation of layer potentials, boundary integral operators, and inverse Fourier transforms of certain singular functions.

#### 3.1 Fourier transform algorithm

Recalling the forward and inverse Fourier transform expressions (2.37) and (2.38), we note that, for smooth and compactly supported functions  $f$ , the corresponding Fourier transforms  $F$  decay superalgebraically fast (i.e., faster than any negative power of  $\omega$ ) as  $\omega \rightarrow \pm\infty$ . Thus, the errors in approximation

$$f(t) \approx \frac{1}{2\pi} \int_{-W}^W F(\omega) e^{-i\omega t} d\omega \quad (3.1)$$

decays super-algebraically fast as  $W \rightarrow \infty$ : the infinite-domain Fourier transform integral can be replaced by the corresponding integral over a finite interval with superalgebraically small errors. As is known [42,49], however, the frequency-domain solutions of the Helmholtz equation in two dimensions vary as an integrable function of  $\log \omega$  which vanishes at  $\omega = 0$ , and, thus, the integration process requires some care to produce the needed integrals with high-order accuracy. To do this, in what follows we employ the recently developed Fourier-continuation (FC) based approach [5] for the numerical evaluation of such singular inverse Fourier transform integrals.

Thus, utilizing a decomposition of the form

$$f(t) = \frac{1}{2\pi} \left( \int_{-W}^{-w_c} + \int_{-w_c}^{w_c} + \int_{w_c}^W \right) F(\omega) e^{-i\omega t} d\omega, \quad (3.2)$$

we only need to consider 1) Integrals of the form

$$I_a^b[F](t) = \int_a^b F(\omega) e^{-i\omega t} d\omega, \quad (3.3)$$

where  $F$  is a smooth non-periodic function, and 2) The half-interval integrals

$$I_0^{w_c}[F](t) = \int_0^{w_c} F(\omega) e^{-i\omega t} d\omega \quad \text{and} \quad I_{-w_c}^0[F](t) = \int_{-w_c}^0 F(\omega) e^{-i\omega t} d\omega, \quad (3.4)$$

where  $F(\omega)$  contains a logarithmic singularity at  $\omega = 0$ .

To treat the integral  $I_a^b[F](t)$ , we re-express it in the form

$$I_a^b[F](t) = e^{-i\delta t} \int_{-A}^A F(\omega + \delta) e^{-i\omega t} d\omega, \quad \delta = \frac{a+b}{2}, \quad A = \frac{b-a}{2}. \quad (3.5)$$

Although  $F(\omega + \delta)$  is not a periodic function of  $\omega$  in the integration interval  $[-A, A]$ , it can be approximated, in this interval, by a Fourier-continuation trigonometric polynomial [20]

$$F(\omega + \delta) = \sum_{m=-\tilde{L}/2}^{\tilde{L}/2-1} c_m e^{i\frac{2\pi}{P}m\omega} \quad (3.6)$$

of a certain periodicity  $P$ , with high-order convergence as  $\tilde{L}$  grows. Indeed, an accurate Fourier approximation of a certain period  $P > 2A$  can be obtained on the basis of the FC(Gram) Fourier Continuation

method [2, 20] from which the approximation errors decay as a user-prescribed negative power of  $\tilde{L}$ . Substituting (3.6) into (3.5) and integrating term-wise gives the approximation

$$\begin{aligned} I_a^b[F](t) &= e^{-i\delta t} \sum_{m=-\tilde{L}/2}^{\tilde{L}/2-1} c_m \int_{-A}^A e^{-i\frac{2\pi}{P}(\alpha t - m)\omega} d\omega \\ &= e^{-i\delta t} \sum_{m=-\tilde{L}/2}^{\tilde{L}/2-1} c_m \frac{P}{\pi(\alpha t - m)} \sin\left(\frac{2\pi A}{P}(\alpha t - m)\right), \end{aligned} \quad (3.7)$$

with errors that are uniform in the time variable  $t$ . For a given user-prescribed equi-spaced time-evaluation grid  $\{t_n = n\Delta t\}_{n=N_1}^{N_2}$ , the quantities  $I_a^b[F](t_n)$  can be obtained via an FFT-accelerated evaluation of scaled discrete convolutions, see Section 4.1.2 in [5] for more details. But here, for simplicity, we evaluate the quantities  $I_a^b[F](t_n)$  directly.

In order to evaluate the integral  $I_0^{w_c}[F](t)$  at fixed cost for arbitrarily times  $t$ , in turn, we utilize a certain modified ‘‘Filon-Clenshaw-Curtis’’ high-order quadrature approach developed in [5] which relies on a graded set

$$\left\{ \mu_j = w_c \left( \frac{j}{Q} \right)^q, j = 1, \dots, Q \right\},$$

of points in the interval  $(0, w_c)$  and associated integration subintervals  $(\mu_j, \mu_{j+1}), j = 1, \dots, Q$ . The integral  $I_0^{w_c}[F](t)$  is thus approximated in accordance with the expression

$$I_0^{w_c}[F](t) = \sum_{j=1}^{Q-1} I_{\mu_j}^{\mu_{j+1}}[F](t),$$

in which the integral  $I_{\mu_j}^{\mu_{j+1}}[F](t)$  is obtained via the Clenshaw-Curtis quadrature rule. This algorithm results in high-order convergence in spite of the logarithmic singular character of the function  $F$ . In detail, letting  $n_{\text{ch}}$  denote the selected number of Clenshaw-Curtis mesh points and assuming that  $q > n_{\text{ch}} + 1$ , the errors resulting from this approximation strategy decay as  $\mathcal{O}(Q^{-(n_{\text{ch}}+1)})$  as  $n_{\text{ch}} \rightarrow +\infty$ .

Algorithm 3 also requires the evaluation of the Fourier transform

$$\mathbb{F}_{k,slow}(f)(\omega) := \int_{-H}^H f(t + s_k) \chi_k(t) e^{i\omega t} dt$$

for the smooth boundary-values function  $f$ . This computation proceeds in a manner analogous to that used for the evaluation of  $I_{w_c}^W[F](t)$ , except that, instead of Fourier continuation approximation of the function  $F$  used in that case, here a regular Fourier expansion

$$f(t + s_k) \chi_k(t) = \sum_{m=-\hat{L}/2}^{\hat{L}/2-1} \hat{c}_m^k e^{i\frac{\pi}{H} m t}, \quad (3.8)$$

of periodicity interval  $[-H, H]$ , is used—which results in high-order convergence on account of the smooth vanishing of the function  $\chi_k(t)$  at the endpoints of the interval  $[-H, H]$ . The approximation of  $\mathbb{F}_{k,slow}(f)(\omega)$  is then obtained via an expression analogous to (3.7), with uniform errors, for all  $\omega \in \mathbb{R}$ , which are determined solely by the error in the approximation (3.8).

### 3.2 Layer-potentials and integral-operator evaluations

The numerical implementation of the hybrid multiple scattering strategy additionally requires evaluation of the layer-potentials  $\mathcal{S}_j$ ,  $j = 1, 2$  and the integral operators  $S_j$ ,  $j = 1, 2$  (equations (2.39) and (2.41), respectively), both of which can be expressed as integrals of the form

$$\mathcal{H}(x, \omega) = \int_{\Gamma_j} \Phi_\omega(x, y) \psi(y, \omega) ds_y, \quad x \in \Gamma_j, \quad \Omega \text{ or } \Gamma \setminus (\Gamma_j), \quad (3.9)$$

for certain densities  $\psi(y, \omega)$ . Depending on the location of observation point  $x$ , the integral  $\mathcal{H}(x, \omega)$  may be weakly-singular, nearly-singular or non-singular. The numerical evaluation of  $\mathcal{H}(x, \omega)$  with high accuracy can be achieved by means of a suitably modified version of the two-dimensional Chebyshev-based rectangular-polar discretization method [22] (cf. [15]) which adequately accounts for the singular character of the unknown potential  $\psi$  at the endpoints of the open-arcs  $\Gamma_j$ . In detail [26], the density function  $\psi$  can be expressed in the forms  $\psi = \alpha/w$  near the endpoints where  $\alpha$  is a smooth function and  $w \sim d_j^{1/2}$  with  $d_j$  denoting the distance to the endpoint of  $\Gamma_j$ . Then a special change of variables introduced in [21, Eq. (4.12)] (see also [3, 18]) can be utilized to evaluate the integrals  $\mathcal{H}(x, \omega)$  with high order of accuracy.

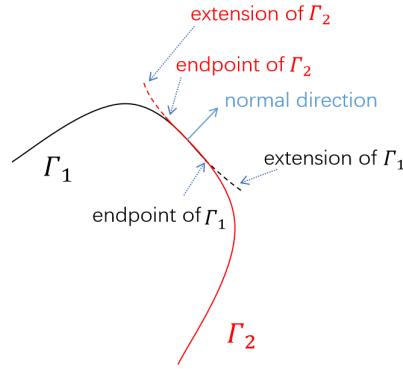


Figure 3: Extended arcs utilized in the numerical implementation.

In view of the aforementioned density singularity, it can be easily shown that the collected boundary data  $F_m$  ( $m \geq 1$ ) is also singular: it behaves like  $d_j^{1/2}$  near the endpoints of the arc  $\Gamma_{j(m)}$ . Graded meshes near the endpoints could be employed to ensure high-order accuracy in the solution of the associated boundary integral equations. But a different approach is utilized in this paper, whereby the edge singularity in the boundary data may be entirely avoided by slightly and smoothly extending the boundary  $\Gamma_j$  in the direction normal to  $\Gamma_j$ —as illustrated in Figure 3. More precisely, letting  $x = x(s)$  and  $\nu = \nu(s)$  denote a parametrization of  $\Gamma_j$  and its normal vector, respectively, the curve  $\Gamma_j$  is prolonged into an extended open arc  $\tilde{\Gamma}_j$ , wherein the extension arc, denoted by  $\Gamma_j^e = \tilde{\Gamma}_j \setminus \Gamma_j$ , is given by

$$y(s) = x(s) + a(s) \cdot \nu(s), \quad y \in \Gamma_j^e, \quad (3.10)$$

where a certain number of derivatives of the function  $a$  are required to vanish at  $s = s_0$ .

This extension provides great flexibility, and it does not negatively affect any aspect of the proposed multiple scattering algorithm. Indeed, considering the wave equation problem (2.3)–(2.5) for the function  $w_j^s$ , but replacing  $\Gamma_j$  and  $\Omega_j$  by  $\tilde{\Gamma}_j$  and  $\tilde{\Omega}_j = \mathbb{R}^2 \setminus \tilde{\Gamma}_j$ , respectively, the proof of Theorem 2.2 can easily be extended to show that under the new assumption

$$g_j(x, t) = 0 \quad \text{for } (x, t) \in (\tilde{\Gamma}_j \times (-\infty, T_0]) \cup ((\Gamma_{12} \cup \Gamma_j^e) \times (-\infty, +\infty)) \quad (3.11)$$



the conclusion of the theorem, namely, equation (2.15), remains valid. Using this modified version of Theorem 2.2, considering the wave equation problem (2.3)-(2.5) with  $\Gamma_{j(m)}$  replaced by  $\tilde{\Gamma}_{j(m)}$ , and replacing the inductive relations (2.24)-(2.25) by

$$f_1(x, t) = -u^i(x, t) \quad \text{on} \quad \tilde{\Gamma}_1, \quad (3.12)$$

and,

$$f_m(x, t) = \begin{cases} -u^i(x, t) - v_1^s(x, t), & x \in \Gamma_{j(m)}, m = 2, \\ -v_{m-1}^s(x, t), & x \in \Gamma_{j(m)}, m \geq 3, \\ 0, & x \in \Gamma_{j(m)}^e, m \geq 2, \end{cases} \quad (3.13)$$

it can easily be checked that the statement and proof of Theorem 2.7 remain valid. Incorporating once again the Fourier transform and time-windowing and recentering strategies introduced in previous sections, we are led to a new version of the hybrid multiple scattering algorithm which, except for straightforward modifications related to arc extensions, is entirely analogous to Algorithm 3, and whose slightly modified pseudocode is therefore omitted for the sake of brevity. The overall algorithm for evaluation of the numerical solution  $u^s$  of equation (2.1), incorporating the extended arcs  $\tilde{\Gamma}_j$  is presented as Algorithm 4 in Section 3.3.

Clearly, the weakly-singular integrals  $\mathcal{H}(x, \omega)$  need to be evaluated at a sufficiently large number of frequency discretization-points  $\omega$  in the interval  $[-W, W]$ . The computational cost required for such evaluations can be reduced by utilizing the decomposition

$$\Phi_\omega(x, y) = \Psi_0(x, y) + \kappa^2 \Psi_1(x, y) + H_\omega(x, y), \quad (3.14)$$

where

$$\Psi_0(x, y) = -\frac{1}{2\pi} \log|x - y|, \quad (3.15)$$

$$\Psi_1(x, y) = \frac{|x - y|^2}{8\pi} \log|x - y|, \quad (3.16)$$

and

$$H_\omega(x, y) = \begin{cases} \Phi_\omega(x, y) - \Phi_0(x, y) - \kappa^2 \Psi_1(x, y), & x \neq y, \\ \frac{i}{4} - \frac{1}{2\pi}(c_e + \log(\kappa/2)), & x = y, \end{cases} \quad (3.17)$$

( $c_e = 0.57721566 \dots$  is the Euler constant). The function  $H_\omega$  is more regular than the Green function  $\Phi_\omega(x, y)$  itself, and its integration under a given error tolerance is therefore less onerous. The discretization matrices associated with the weakly-singular and nearly-singular integrals of the form

$$\mathcal{H}_\ell(x, \omega) = \int_{\tilde{\Gamma}_j} \Psi_\ell(x, y) \psi(y, \omega) ds_y, \quad x \in \tilde{\Gamma}_j, \quad \Omega \text{ or } \Gamma \setminus (\tilde{\Gamma}_j), \quad \ell = 0, 1, \quad (3.18)$$

in turn, are independent of frequency, and can thus be precomputed before the ping-pong iterative process is initiated.

In this work, the two-dimensional Chebyshev-based rectangular-polar integral solver [15, 22] is employed for the evaluation of all singular integrals. The remaining integrals involving the smoother kernels  $H_\omega$  can be integrated efficiently and accurately by means of Fejer's quadrature rule, and they can be further accelerated e.g. by the methods presented in [11, 19, 40] and references therein, but such accelerations were not utilized in this work. In our numerical implementation, prior to the ping-pong iteration process we additionally use

the Lapack function ZGESV to pre-compute the inverses  $\mathbb{A}_j^{-1}(\omega)$  of the coefficient matrixes  $\mathbb{A}_j(\omega)$  ( $j = 1, 2$ ) resulting from the discretizations of the integral operators

$$\mathcal{H}_1(x, \omega) + \mathcal{H}_2(x, \omega) + \int_{\tilde{\Gamma}_j} H_\omega(x, y) \psi(y, \omega) ds_y, \quad x \in \tilde{\Gamma}_j, \quad j = 1, 2; \quad (3.19)$$

these inverse matrices are then used repeatedly to obtain the numerical solution  $\psi_{m,k}(x, \omega)$  of the integral equation (2.50) with  $j = j(m)$  for all  $k \in \mathcal{K}$  and all  $m = 1, \dots, M$ .

### 3.3 Numerical implementation: overall outline

The overall algorithm for evaluation of the numerical solution  $u^s$  of equation (2.1) relies on the concepts presented in Sections 3.1-3.2 and the following notations and conventions.

With reference to Section 3.1, we denote by  $\mathcal{F} = \{\omega_1, \dots, \omega_J\}$  a set of frequencies used for the Fourier transformation process, which includes an equi-spaced grid in the frequency intervals  $[-W, -w_c]$  and  $[w_c, W]$ , as well as a combination of the Clenshaw-Curtis mesh points in the intervals  $(-\mu_{j+1}, -\mu_j)$  and  $(\mu_j, \mu_{j+1})$ ,  $j = 1, \dots, Q - 1$ , for a total of  $J = 2\tilde{L} + 2n_{\text{ch}}(Q - 1)$  frequency discretization points. For the necessary time-domain discretization, in turn, we use the mesh  $\mathcal{T} = \{t_n = n\Delta t\}_{n=1}^{N_T}$  of the time interval  $[0, s_K + H]$ , where  $\Delta t = (s_K + H)/N_T$ , and we call  $\mathcal{T}_0 = \mathcal{T} \cap [0, T]$ . With reference to Section 3.2, on the other hand, frequency-independent meshes  $\mathcal{C}_j$  are used on the curves  $\tilde{\Gamma}_j$ ,  $j = 1, 2$  for all frequencies considered. The set of discrete spatial observation points at which the scattered field is to be produced, finally, is denoted by  $\mathcal{R}$ .

Using these notations, a version of Algorithm 3, including certain details concerning our numerical implementation, is presented in Algorithm 4.

---

#### Algorithm 4 Numerical hybrid multiple scattering algorithm with time-recentering

---

- 1: Pre-compute the matrices  $\mathbb{A}_j^{-1}(\omega)$  for  $j = 1, 2$ ,  $\omega \in \mathcal{F}$ .
- 2: Do  $m = 1, 2, \dots, M$
- 3:     Evaluate the boundary data  $f_m(x, t)$ ,  $(x, t) \in \mathcal{C}_{j(m)} \times \mathcal{T}$  via relations (3.12)-(3.13).
- 4:     Initialize  $v_m^s(x, t) = 0$ ,  $(x, t) \in (\mathcal{R} \times \mathcal{T}_0) \cup (\mathcal{C}_{j(m)} \times \mathcal{T})$ .
- 5:     Do  $k = 1, 2, \dots, K$
- 6:         For  $\omega \in \mathcal{F}$ , evaluate the vectors  $\mathbb{B}_{m,k}(\omega)$  whose elements are

$$F_{m,k}(x, \omega) = \mathbb{F}_{k, \text{slow}}(f_m)(x, \omega), \quad x \in \mathcal{C}_{j(m)},$$

by the Fourier transform algorithm presented in Section 3.1.

- 7:     Compute the approximation of the solution  $\psi_{m,k}(x, \omega)$ ,  $(x, \omega) \in \mathcal{C}_{j(m)} \times \mathcal{F}$  of the integral equation (2.50) given by  $\mathbb{A}_j^{-1}(\omega)\mathbb{B}_{m,k}(\omega)$ .
- 8:     Evaluate  $V_{m,k}^s(x, \omega)$ ,  $(x, \omega) \in (\mathcal{R} \cup \mathcal{C}_{j(m)}) \times \mathcal{F}$  through (2.49) and rectangular-polar Chebyshev-based integration (Section 3.2).
- 9:     Evaluate  $v_m^s(x, t) = v_m^s(x, t) + \mathbb{F}^{-1}(V_{m,k}^s)(x, t - s_k)$ ,  $(x, t) \in (\mathcal{R} \times \mathcal{T}_0) \cup (\mathcal{C}_{j(m)} \times \mathcal{T})$  by the Fourier transform algorithm presented in Section 3.1.
- 10:    End Do
- 11: End Do
- 12: Evaluate the numerical solution

$$u_{\text{num}}^s(x, t) = \sum_{m=1}^M v_m^s(x, t), \quad (x, t) \in \mathcal{R} \times \mathcal{T}_0. \quad (3.20)$$


---

## 4 Numerical examples

This section presents a variety of numerical tests that illustrate the character of the proposed frequency-time hybrid ping-pong integral-equation solver embodied in Algorithm 4. The numerical errors presented in this section were calculated in accordance with the expression  $\max_{t \in [0, T]} |u_{\text{num}}^s - u_{\text{ref}}^s|$  where, with exception of the test case considered in Example 3, for which the exact solution is known, the reference solution  $u_{\text{ref}}^s$  was obtained as a numerical solution for sufficiently fine discretizations. (Our use of absolute errors is justified since, as evident from the numerical solution plots in each case, we only consider solutions whose maximum values are quantities of order one.) All of the numerical tests were obtained on the basis of Fortran numerical implementations, parallelized using OpenMP, on an 10-core HP Desktop with an Intel Core processor i9-10900.

**Example 1.** Our first test case concerns the accuracy of the numerical solver for the frequency domain integral equation (2.40) on the single open-arc  $\Gamma_1$  shown in Figure 1(c), with point-source boundary data

$$F_1 = -U^i = -\frac{i}{4}H_0^{(1)}(\kappa|x|) \quad \text{on } \Gamma_1. \quad (4.1)$$

Figure 4 displays errors in the solution evaluated by means of the single-layer potential (2.39), at the points  $(0.5, 0)$ ,  $(0, 2)$ ,  $(0, 1.01)$ ,  $(-0.99, 0)$ , as functions the number  $N$  of Chebyshev points used in each one of the patches associated with the Chebyshev-based discretization methodology [22]. Clearly, uniform fast convergence of the numerical solutions is obtained at all points, independently of the distance to the boundary. For this example a total of 5 patches (resp. 25 patches) were used for test cases with wavenumber  $\kappa = 10$  (resp.  $\kappa = 50$ ).

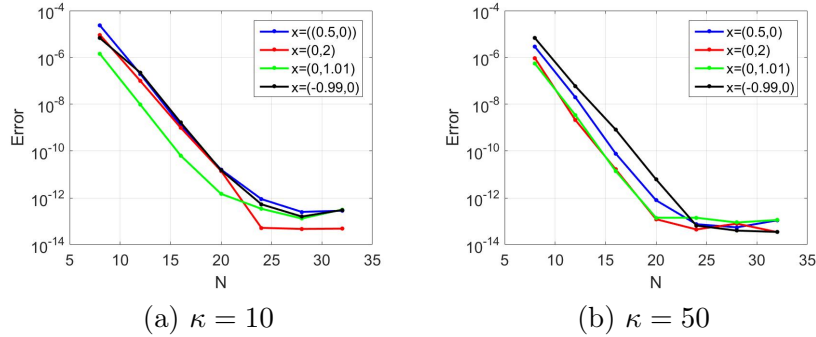


Figure 4: Numerical errors observed in the frequency-domain solutions considered in Example 1, at various points  $x$ , as functions of the number  $N$  of discretization points used.

**Example 2.** We now consider test cases that demonstrates the accuracy of the *time-domain* solver for the problem scattering by a single open-arc  $\Gamma_1$  depicted in Figure 1(c). We consider incident fields of two different kinds, namely, 1) A Gaussian-modulated point source  $u_1^i(x, t)$  equal to the Fourier transform of the function

$$U^i(x, \omega) = \frac{5i}{2}H_0^{(1)}(\omega|x-z|)e^{-\frac{(\omega-\omega_0)^2}{\sigma^2}}e^{i\omega t_0} \quad (4.2)$$

with respect to  $\omega$ , with  $\sigma = 2$ ,  $\omega_0 = 15$ ,  $t_0 = 4$  and  $z = (0, 0)$ ; and 2) A plane-wave incident field

$$u_2^i(x, t) = -\sin(4g(x, t))e^{-1.6(g(x, t)-3)^2}, \quad g(x, t) = t - t_{\text{lag}} - x \cdot d^{\text{inc}} \quad (4.3)$$

along the incident direction  $d^{\text{inc}} = (1, 0)$  with  $t_{\text{lag}} = 2$ . Together with a sufficiently fine fixed spatial discretization, the fixed numerical frequency intervals  $\omega \in [5, 25]$  and  $\omega \in [-20, 20]$  were used for the

incident fields  $u_1^i$  and  $u_2^i$ , respectively. Figures 5 and 6 presents the time trace of the scattered field at the observation point  $x = (0.5, 0)$  and the corresponding numerical errors at that point as a function of the number of frequencies used—demonstrating the fast convergence of the algorithms as the frequency-domain discretization is refined.

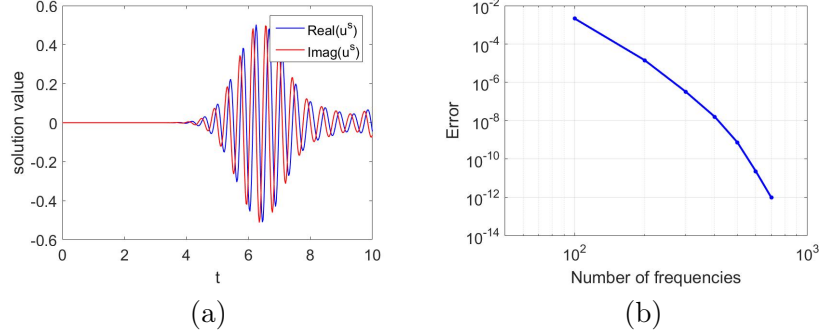


Figure 5: Scattered field and errors obtained for the problem considered in Example 2. (a) Real and imaginary parts of scattered field at  $x = (0.5, 0)$  resulting from the incident field  $u_1^i$ . (b) Convergence of the complex scattered field at  $x = (0.5, 0)$  as a function of the number of frequencies used.

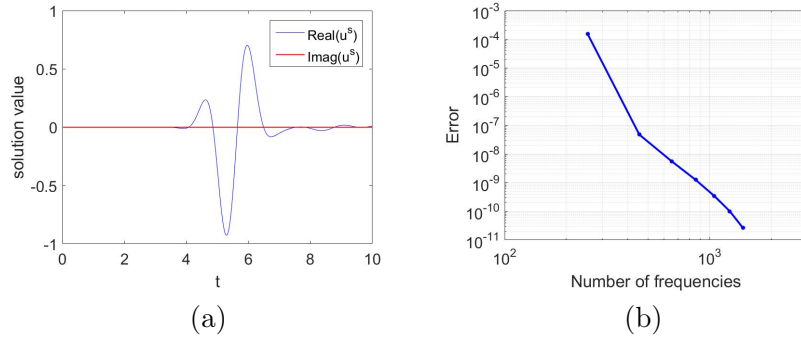


Figure 6: Scattered field and errors obtained for the problem considered in Example 2. (a) Real and imaginary parts of scattered field at  $x = (0.5, 0)$  resulting from the incident field  $u_2^i$ . (b) Convergence of the complex scattered field at  $x = (0.5, 0)$  as a function of the number of frequencies used.

**Example 3.** This example presents the solutions produced by the full hybrid ping-pong multiple scattering algorithm for the wave equation problem (2.1) in two different domains  $\Omega$ , namely, the unit disc centered at the origin and the unit square  $\Omega = [-1, 1]^2$ , for  $t \in [0, 10]$ , and for each one of the two time-domain sources considered in Example 2: the point source  $u_1^i(x, t)$  and the plane wave source  $u_2^i(x, t)$ . For the plane-wave incidence case the exact solution is given by  $u^s(x, t) = -u_2^i(x, t)$  for  $x \in \Omega$ . In this example, the extensions  $\tilde{\Gamma}_j$  of  $\Gamma_j$  for  $j = 1, 2$  are constructed by means of portions of tangent circular arcs of radii 0.1. For the wave equation problem (2.1) in a unit disc domain, the numerical errors as a function of  $M$  are displayed in Figure 7 and 8: clearly, rapid convergence and high accuracy are observed. Figures 9 and 10 display the total field within the rectangular domain  $\Omega$  at various times, for two different point-source locations  $z$ , and two different values of  $\omega_0$  in (4.2), and using a total of  $M = 10$  ping-pong iterations; we have verified that, in this case, the numerical errors are less than  $10^{-8}$  for all  $t \in [0, 10]$ .

**Example 4.** We now use Algorithm 4 to solve wave equation problems in a disc-shaped domain (Figure 1(c)) and a T-shaped domain (Figure 11(a)), up to final times  $T = 10$ , and using  $M = 7$  ping-pong iterations. The incident wave is a pulse function given by

$$u^i(x, t) = f(t - |x - z_0|/c), \quad f(s) = \sin(4s)e^{-1.6(s-3)^2}, \quad (4.4)$$

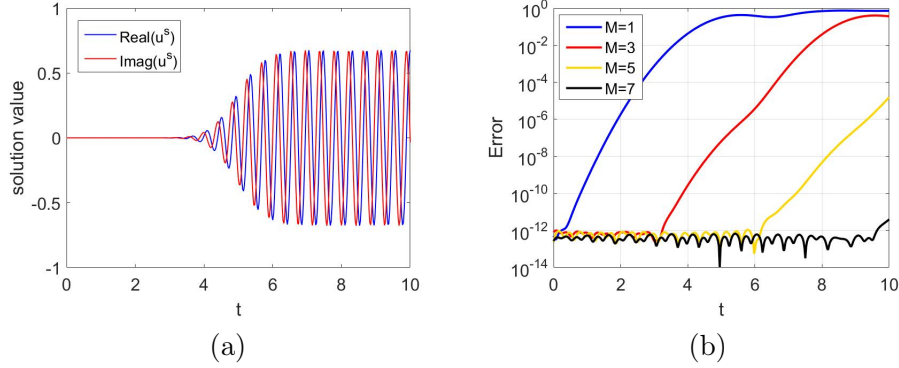


Figure 7: Scattered field and errors obtained for the problem considered in Example 3. (a) Real and imaginary parts of scattered field at  $x = (0.5, 0)$  resulting from the incident field  $u_1^i$ . (b) Numerical errors as functions of time  $t$  for various values of  $M$ .

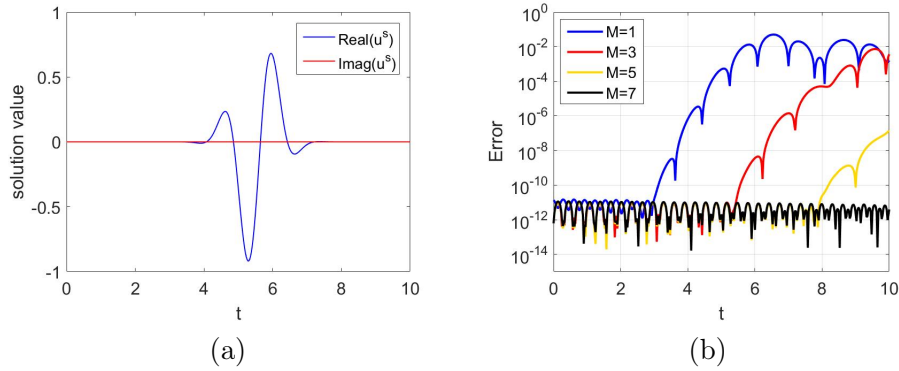


Figure 8: Scattered field and errors obtained for the problem considered in Example 3. (a) Real and imaginary parts of scattered field at  $x = (0.5, 0)$  resulting from the incident field  $u_2^i$ . (b) Numerical errors as functions of time  $t$  for various values of  $M$ .

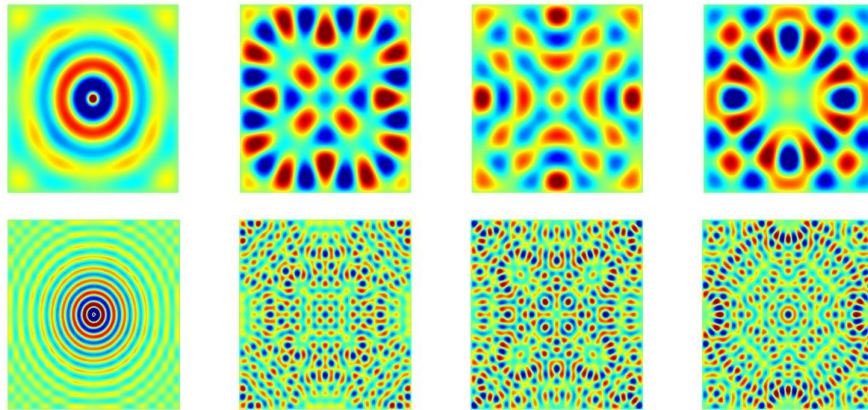


Figure 9: Real part of the total fields for the problem considered in Example 3 with point source located at  $z = (0, 0)$ . Upper row:  $\omega_0 = 15$ . Lower row:  $\omega_0 = 50$ . Fields at times  $t = 4, 6, 8$  and  $10$  are displayed from left to right in each row.

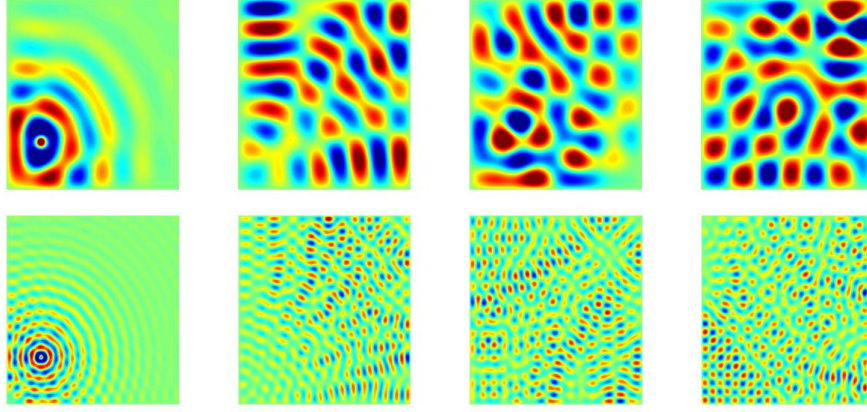
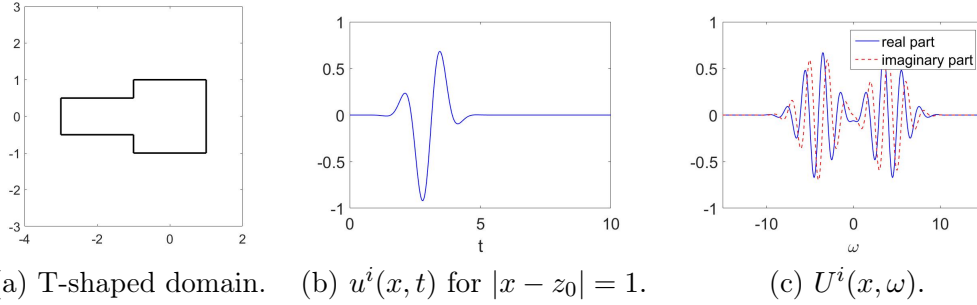


Figure 10: Real part of the total fields for the problem considered in Example 3 with point source located at  $z = (-0.6, -0.5)$ . Upper row:  $\omega_0 = 15$ . Lower row:  $\omega_0 = 50$ . Fields at times  $t = 4, 6, 8$  and  $10$  are displayed from left to right in each row.

which is displayed in Figure 11(b). Figure 11(c) displays the corresponding Fourier transform, in view of which the fixed numerical bandwidth value  $W = 15$  was used for this example. Figures 12-14 display the total field within  $\Omega$  at various times and for different source point locations.



(a) T-shaped domain. (b)  $u^i(x, t)$  for  $|x - z_0| = 1$ . (c)  $U^i(x, \omega)$ .

Figure 11: Setup utilized for the test case considered in Example 4, including, (a) The T-shaped domain used, as well as, (b) The time-domain incident wave  $u^i(x, t)$ , and, (c) Its Fourier transform  $U^i(x, \omega)$ . The Fourier transform displayed in (c) is smaller than  $10^{-8}$  outside the  $\omega$ -range considered in the figure.

**Example 5.** This final example concerns a long time propagation and scattering problem in a unit disc domain under the incident wave (4.4) with  $z_0 = (0, 0)$ . For this example we have used  $\delta_{12} = 2 \sin \frac{\pi}{10} \approx 0.618$ ,  $M = 45$ ,  $K = 4$  (so that  $s_K + H = 55$ ),  $W = 20$ ,  $J = 454$ , and  $\Delta t = 0.11$ , and we have computed the necessary frequency domain solutions using open-arc discretizations  $\mathcal{C}_j, j = 1, 2$ , each one of which contains 224 discretization points. Note that the exact solution values at the points  $x = (-\sqrt{3}/4, 1/4)$  and  $x = (0.5, 0)$  coincide (since  $|(-\sqrt{3}/4, 1/4)| = |(0.5, 0)| = 0.5$ ). This simple symmetry relation provides a valuable verification of the numerical solution—which, as illustrated Figure 15, is closely satisfied by the numerical solution. Tables 2 and 3, finally, present the numerical solution errors for the present problem at the point  $x = (0.5, 0)$ , for various values of  $M$  and corresponding final times  $T(M)$ , together with other statistics such as precomputation time and total computational times. Note in particular that the solution errors do not grow as the final times increase.

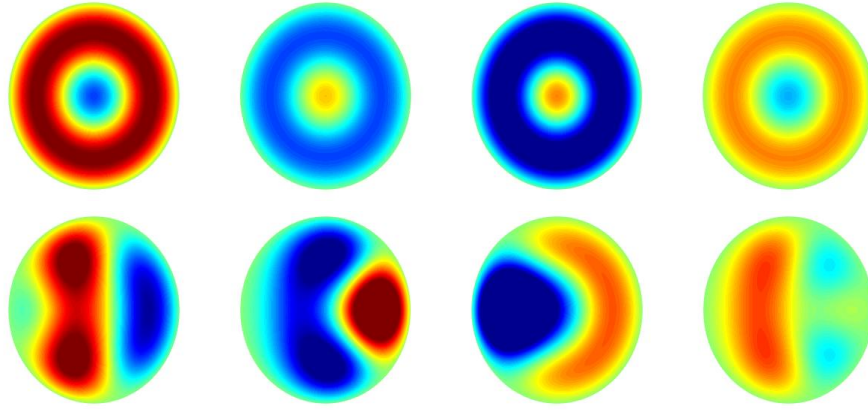


Figure 12: Total fields in the disc-shaped domain considered in Example 4. Upper row:  $z_0 = (0, 0)$ . Lower row:  $z_0 = (-0.5, 0)$ . Fields at times  $t = 4, 6, 8$  and  $10$  are displayed from left to right in each row.

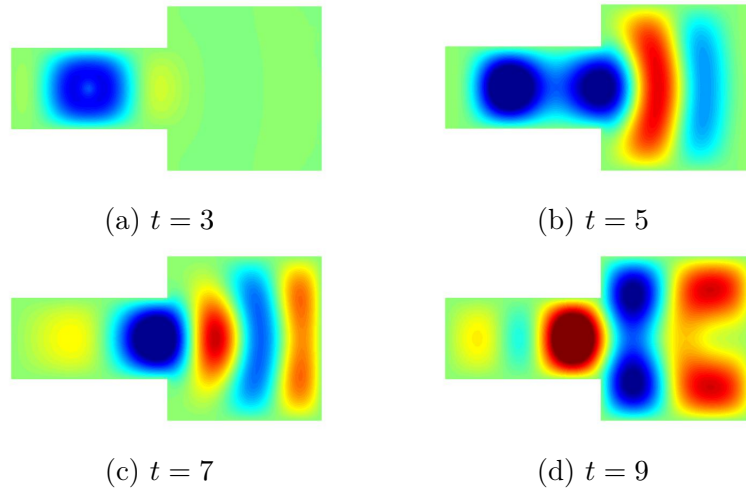


Figure 13: Total fields in the T-shaped domain considered in Example 4, with point source located at  $z_0 = (-2, 0)$ , at various times  $t$ .

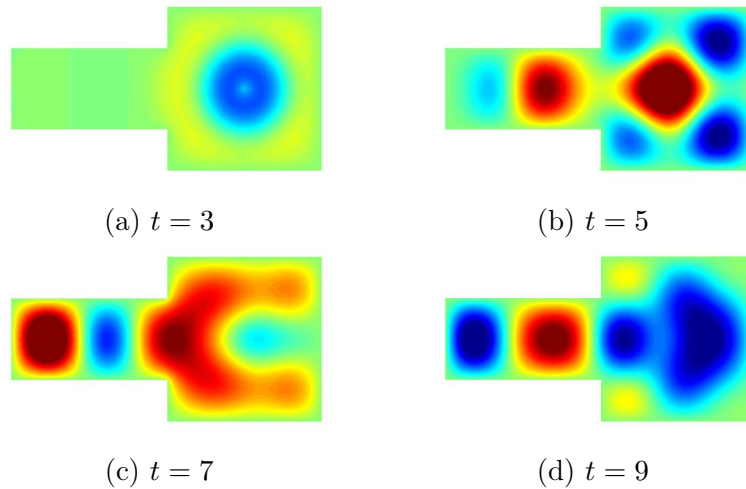


Figure 14: Total fields in the T-shaped domain considered in Example 4, with point source located at  $z_0 = (0, 0)$ , at various times  $t$ .

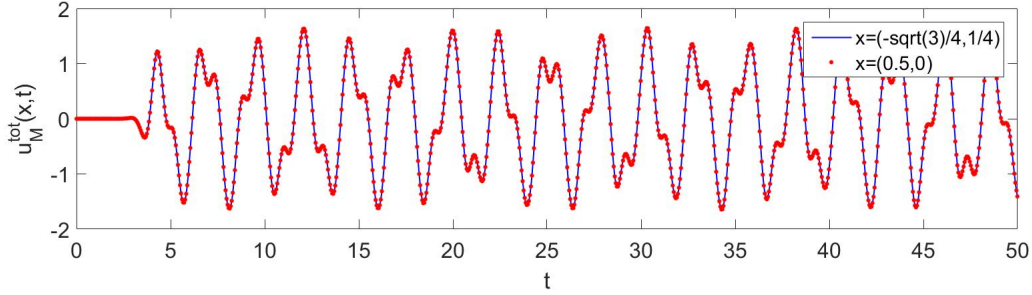


Figure 15: Time-domain solutions  $u_M^{tot}(x, t), t \in [0, 50]$  considered in Example 5 at  $x = (-\sqrt{3}/4, 1/4)^\top$  and  $x = (0.5, 0)^\top$  with  $M = 45$ . As illustrated in the figure, these two time traces coincide, by symmetry.

Table 2: Numerical errors, precomputation time and total computational times required by the problem considered in Example 5 for various values of  $M$ .  $J = 254$  frequencies were used in all cases.

$M$	15	25	35	45
$T(M)$	8.652	14.832	21.012	27.192
Error ( $t \in [0, T(M)]$ )	$6.57 \times 10^{-4}$	$4.74 \times 10^{-5}$	$1.87 \times 10^{-5}$	$5.56 \times 10^{-6}$
Time (precomputation)	9.1 s			
Time ( $M$ iterations)	30.0 s	52.2 s	73.1 s	94.4 s

## 5 Conclusions

This paper proposed a frequency-time hybrid integral-equation method for the wave equation problem in an interior two-dimensional bounded spatial domain. The solver is based on a novel ping-pong multiple scattering strategy that reduces the original problem to a sequence of problems of scattering by open-arcs. Exploiting the Huygens principle, relying on a domain decomposition strategy based on use of overlapping patches, and utilizing boundary integral equation formulations for frequency-domain sub-problems and an efficient Fourier transform algorithm, the proposed method produces the interior time-domain solution efficiently and with high accuracy. An extension of the ping-pong algorithm that incorporates arbitrary numbers of overlapping subdomains should enable application of the method to complex 2D and 3D geometries. The method can also be extended to enable solution of elastic and electromagnetic wave problems, and including problems of scattering by impenetrable obstacles and problem of transmission for penetrable structures. Such extensions, which lie beyond the scope of this paper, are left for future work.

## Acknowledgments

OB gratefully acknowledges support from NSF, DARPA and AFOSR through contracts DMS-2109831, HR00111720035, FA9550-19-1-0173 and FA9550-21-1-0373, and by the NSSEFF Vannevar Bush Fellowship

Table 3: Numerical errors, precomputation time and total computational times required by the problem considered in Example 5 for various values of  $M$ .  $J = 454$  frequencies were used in all cases.

$M$	15	25	35	45
$T(M)$	8.652	14.832	21.012	27.192
Error ( $t \in [0, T(M)]$ )	$1.24 \times 10^{-7}$	$2.59 \times 10^{-8}$	$1.10 \times 10^{-8}$	$4.36 \times 10^{-9}$
Time (precomputation)	16.8 s			
Time ( $M$ iterations)	46.3 s	78.4 s	109.8 s	141.3 s



under contract number N00014-16-1-2808. TY gratefully acknowledges support from NSFC through Grant No. 12171465.

## A Appendix

This appendix establishes the explicit expression (2.21) for the solutions  $v^s(x, t)$  of problem (2.16) used in the proof of Lemma 2.3. To do this we recall from Section 2.3 that, for  $x \in \mathbb{R}^2 \setminus \overline{B_R}$ ,  $v^s(x, t)$  equals the inverse Fourier transform of

$$V^s(x, \omega) = \int_{\Gamma} \partial_{\nu_y} G_{\omega}(x, y) F(y, \omega) ds_y, \quad x \in \mathbb{R}^2 \setminus \overline{B_R},$$

with respect to  $\omega$ , where

$$\partial_{\nu_y} G_{\omega}(x, y) = \frac{i\kappa |x|^2 - R^2}{4R} H_1^{(1)}(\kappa|x - y|),$$

and we introduce the following notations. We call  $\check{\Gamma} = \Gamma \times (-\infty, +\infty)$  the cylindrical boundary in three dimensional space with cross-section  $\Gamma$ , we let  $\check{x} = (x^\top, 0)^\top \notin \check{\Gamma}$ ,  $\check{y} = (y^\top, z)^\top \in \check{\Gamma}$  and  $\check{r} = \sqrt{r^2 + z^2}$  with  $r = |x - y| = \sqrt{(x_1 - y_1)^2 + (x_2 - y_2)^2}$ . Using the unit normal  $\nu_y$  of  $\Gamma$ , finally, the corresponding unit normal on  $\check{\Gamma}$  is denoted by  $\check{\nu}_{\check{y}} = (\nu_y^\top, 0)^\top$ .

In preparation for the main result of this appendix we establish the following Lemma.

**Lemma A.1.** *The following formulas hold:*

$$\frac{1}{4\pi} \int_{-\infty}^{\infty} \frac{e^{i\kappa\check{r}}}{\check{r}} dz = \frac{i}{4} H_0^{(1)}(\kappa r), \quad (\text{A.1})$$

$$\frac{1}{4\pi} \int_{-\infty}^{\infty} \partial_{y_i} \left( \frac{e^{i\kappa\check{r}}}{\check{r}} \right) dz = \frac{i}{4} \partial_{y_i} H_0^{(1)}(\kappa r), \quad i = 1, 2. \quad (\text{A.2})$$

*Proof.* The expression (A.1) is established in [24, Lemma 3.1]. Using the notations

$$\check{r}_0 = (x_1^2 + (x_2 - y_2)^2 + z^2)^{1/2},$$

to establish the  $y_1$  component of (A.2) (the  $y_2$  component follows analogously), it suffices to show that

$$\int_0^{y_1} dy_1 \int_1^{\infty} \partial_{y_1} \left( \frac{e^{i\kappa\check{r}}}{\check{r}} \right) dz = \int_1^{\infty} \frac{e^{i\kappa\check{r}}}{\check{r}} dz - \int_1^{\infty} \frac{e^{i\kappa\check{r}_0}}{\check{r}_0} dz; \quad (\text{A.3})$$

the result then follows by differentiation with respect to  $y_1$ . To establish (A.3), we seek to utilize the Fubini's Theorem on the left hand integral, but, unfortunately, the integrand does not satisfy the hypothesis of Fubini's theorem: it is not an integrable function of the variable  $(y_1, z)$ . To address this difficulty we integrate by parts the left-hand integral: using the relation

$$e^{i\kappa\check{r}} = \frac{\check{r}}{i\kappa z} \partial_z e^{i\kappa\check{r}}, \quad (\text{A.4})$$

we obtain

$$\int_1^{\infty} \partial_{y_1} \left( \frac{e^{i\kappa\check{r}}}{\check{r}} \right) dz = \int_1^{\infty} \frac{1}{i\kappa z} \partial_z \partial_{y_1} e^{i\kappa\check{r}} dz = -\frac{1}{i\kappa} \partial_{y_1} e^{i\kappa\check{r}} \Big|_{z=1} + \int_1^{\infty} \frac{1}{i\kappa z^2} \partial_{y_1} e^{i\kappa\check{r}} dz.$$

The Fubini's Theorem can now be applied to the integrand to the last integrand, and we thus obtain

$$\begin{aligned} \int_0^{y_1} dy_1 \int_1^\infty \partial_{y_1} \left( \frac{e^{i\kappa\check{r}}}{\check{r}} \right) dz &= -\frac{1}{i\kappa} e^{i\kappa\check{r}} \Big|_{z=1} + \frac{1}{i\kappa} e^{i\kappa\check{r}_0} \Big|_{z=1} + \int_0^{y_1} dy_1 \int_1^\infty \frac{1}{i\kappa z^2} \partial_{y_1} e^{i\kappa\check{r}} dz \\ &= -\frac{1}{i\kappa} e^{i\kappa\check{r}} \Big|_{z=1} + \frac{1}{i\kappa} e^{i\kappa\check{r}_0} \Big|_{z=1} + \int_1^\infty \frac{1}{i\kappa z^2} (e^{i\kappa\check{r}} - e^{i\kappa\check{r}_0}) dz. \end{aligned}$$

Now, replacing  $z^{-2} = -\partial_z z^{-1}$  and integrating by parts in the last integral, and then using (A.4) once again equation (A.3) results, as desired. The proof is now complete.  $\square$

To establish (2.21) we proceed as follows. In view of Lemma A.1 and equation (2.19), and noting that for  $x \in \mathbb{R}^2 \setminus \overline{B_R}, y \in \Gamma$  we have  $x_1 - y_1 \neq 0$  or  $x_2 - y_2 \neq 0$ , the normal derivative of the Green function on the boundary of the circle is given by

$$\begin{aligned} \partial_{\nu_y} G_\omega(x, y) &= \frac{i\kappa |x|^2 - R^2}{4R} H_1^{(1)}(\kappa r) \\ &= \frac{i}{4} \frac{|x|^2 - R^2}{R} \frac{r}{x_i - y_i} \partial_{y_i} H_0^{(1)}(\kappa r) \quad (x_i - y_i \neq 0) \\ &= \frac{1}{4\pi} \frac{|x|^2 - R^2}{R} \frac{r}{x_i - y_i} \int_{-\infty}^\infty \partial_{y_i} \left( \frac{e^{i\kappa\check{r}}}{\check{r}} \right) dz \\ &= -\frac{1}{4\pi} \frac{|x|^2 - R^2}{R} r \int_{-\infty}^\infty \frac{i\kappa\check{r} - 1}{\check{r}^3} e^{i\kappa\check{r}} dz \end{aligned}$$

and, therefore, equation (2.20) gives

$$V^s(x, \omega) = -\frac{1}{4\pi} \frac{|x|^2 - R^2}{R} \int_{\check{\Gamma}} \frac{i\kappa\check{r} - 1}{\check{r}^3} r e^{i\kappa\check{r}} F(y, \omega) ds_{\check{y}}, \quad x \in \mathbb{R}^2 \setminus \overline{B_R}.$$

Taking the inverse Fourier transform we obtain

$$\begin{aligned} v^s(x, t) &= \frac{1}{4\pi} \frac{|x|^2 - R^2}{R} \int_{\check{\Gamma}} \int_0^t \left[ \frac{r}{\check{r}^3} \delta(t - \tau - c^{-1}\check{r}) + \frac{r}{c\check{r}^2} \delta'(t - \tau - c^{-1}\check{r}) \right] f(y, \tau) d\tau ds_{\check{y}} \\ &= \frac{1}{4\pi} \frac{|x|^2 - R^2}{R} \int_{\check{\Gamma}} \left[ \frac{r}{\check{r}^3} f(y, t - c^{-1}\check{r}) + \frac{r}{c\check{r}^2} f^{(1)}(y, t - c^{-1}\check{r}) \right] ds_{\check{y}}. \end{aligned}$$

where  $f^{(1)}(x, t) = \frac{\partial f}{\partial t}(x, t)$ . Using the relations  $ds_{\check{y}} = dz ds_y$  and  $\check{\Gamma} = \Gamma \times \mathbb{R}$  we thus obtain

$$\begin{aligned} v^s(x, t) &= \frac{1}{2\pi} \frac{|x|^2 - R^2}{R} \int_{\Gamma} r \int_0^{+\infty} \left[ (r^2 + z^2)^{-3/2} f(y, t - c^{-1}\sqrt{r^2 + z^2}) \right. \\ &\quad \left. + \frac{1}{c(r^2 + z^2)} f^{(1)}(y, t - c^{-1}\sqrt{r^2 + z^2}) \right] dz ds_y. \end{aligned}$$

Utilizing the change of variables  $\tau = t - c^{-1}\sqrt{r^2 + z^2}$ , or equivalently  $z = c\sqrt{(t - \tau)^2 - c^{-2}r^2}$ , and  $dz = -cz^{-1}\sqrt{r^2 + z^2}d\tau$ , we then obtain

$$(r^2 + z^2)^{-3/2} dz = -\frac{1}{c^2(t - \tau)^2 \sqrt{(t - \tau)^2 - c^{-2}r^2}} d\tau$$

and

$$\frac{1}{c(r^2 + z^2)} dz = -\frac{1}{c^2(t - \tau) \sqrt{(t - \tau)^2 - c^{-2}r^2}} d\tau.$$

It then follows that, for  $x \in \mathbb{R}^2 \setminus \overline{B_R}$ ,

$$v^s(x, t) = \frac{1}{2\pi c^2 R} \int_{\Gamma} \int_0^{t-c^{-1}|x-y|} \left[ \frac{|x-y|(|x|^2 - R^2)f(y, \tau)}{(t-\tau)^2 \sqrt{(t-\tau)^2 - c^{-2}|x-y|^2}} + \frac{|x-y|(|x|^2 - R^2)f^{(1)}(y, \tau)}{(t-\tau) \sqrt{(t-\tau)^2 - c^{-2}|x-y|^2}} \right] d\tau ds_y,$$

and, finally, using the assumption (2.17), that

$$v^s(x, t) = \frac{1}{2\pi c^2 R} \int_{\Gamma^{\text{inc}}} \int_0^{t-c^{-1}|x-y|} \left[ \frac{|x-y|(|x|^2 - R^2)f(y, \tau)}{(t-\tau)^2 \sqrt{(t-\tau)^2 - c^{-2}|x-y|^2}} + \frac{|x-y|(|x|^2 - R^2)f^{(1)}(y, \tau)}{(t-\tau) \sqrt{(t-\tau)^2 - c^{-2}|x-y|^2}} \right] d\tau ds_y \quad (\text{A.5})$$

which establishes (2.21), as desired.

**Remark A.2.** *Although not used in this paper, it is worthwhile to note here that, for an arbitrary two-dimensional Lipschitz curve, and letting, as above,  $\tilde{\Gamma} = \Gamma \times \mathbb{R}$ , the change of variables used in this appendix can easily be utilized to obtain an expression for the time-domain double-layer potential in two-dimensions, which had heretofore not been successfully derived. Utilizing the same notations above, from the Kirchhoff formula [47, Eq. (22), Sec. 8.1], we know that the classical three-dimensional time-domain double-layer potential is given by*

$$\mathcal{D}_{3D}(\phi)(\check{x}, t) = \frac{1}{4\pi} \int_{\tilde{\Gamma}} \left[ \frac{\partial(\check{r}^{-1})}{\partial \nu_{\check{y}}} \phi(\check{y}, t - c^{-1}\check{r}) - \frac{1}{c\check{r}} \frac{\partial \check{r}}{\partial \nu_{\check{y}}} \phi^{(1)}(\check{y}, t - c^{-1}\check{r}) \right] ds_{\check{y}}.$$

The two-dimensional double-layer potential  $\mathcal{D}_{2D}$  can then be obtained by assuming that the causal signal  $\phi$  is independent of  $z$ . Then using the change of variables  $\tau = t - c^{-1}\sqrt{r^2 + z^2}$  introduced above we obtain

$$\begin{aligned} & \mathcal{D}_{2D}(\phi)(x, t) \\ &= \frac{1}{2\pi c^2} \int_{\Gamma} \int_0^{t-c^{-1}|x-y|} \left[ \frac{(x-y) \cdot \nu_y \phi(y, \tau)}{(t-\tau)^2 \sqrt{(t-\tau)^2 - c^{-2}|x-y|^2}} + \frac{(x-y) \cdot \nu_y \phi^{(1)}(y, \tau)}{(t-\tau) \sqrt{(t-\tau)^2 - c^{-2}|x-y|^2}} \right] d\tau ds_y. \end{aligned}$$

which provides a correction to the expression presented in [45, Page 19]. The contributions [9, Sections 6.3-6.5], [34, Page 42] and references therein outline some of the difficulties previously encountered with regard to the 2D double-layer potential.

## References

- [1] B. Alpert, L. Greengard, T. Hagstrom, Nonreflecting boundary conditions for the time-dependent wave equation, J. Comput. Phys. 180 (2002) 270-296.
- [2] F. Amlani, O.P. Bruno, An FC-based spectral solver for elastodynamic problems in general three-dimensional domains, J. Comput. Phys. 307 (2016) 333-354.
- [3] K.E. Atkinson, I.H. Sloan. The numerical solution of first-kind logarithmic-kernel integral equations on smooth open arcs. Math. Comp. 56 (1991) 119-139.
- [4] T.G. Anderson, Hybrid Frequency-Time Analysis and Numerical Methods for Time-Dependent Wave Propagation (Ph.D. thesis), California Institute of Technology, 2020.

- [5] T.G. Anderson, O.P. Bruno, M. Lyon, High-order, dispersionless “fast-hybrid” wave equation solver. Part I:  $O(1)$  sampling cost via incident-field windowing and recentering, *SIAM J. Sci. Comput.* 422 (2020) A1348-A1379.
- [6] I.M. Babuška, S.A. Sauter, Is the pollution effect of the FEM avoidable for the Helmholtz equation considering high wave numbers? *SIAM J. Numer. Anal.* 34 (1997) 2392-2423.
- [7] A. Bamberger, T. Ha-Duong, Formulation variationnelle espace-temps pour le calcul par potentiel retardé de la diffraction d’une onde acoustique, *Math. Methods Appl. Sci.* 8 (1986) 405-435.
- [8] L. Banjai, M. Kachanovska, Fast convolution quadrature for the wave equation in three dimensions, *J. Comput. Phys.* 279 (2014) 103-126.
- [9] B.B. Baker, E.T. Copson, *The Mathematical Theorey Huygens’ Principle*, Oxford at the Clarendon Press, 1939.
- [10] A.H. Barnett, L. Greengard, T. Hagstrom, High-order discretization of a stable time-domain integral equation for 3D acoustic scattering, *J. Comput. Phys.* 402 (2020) 109047.
- [11] C. Bauinger, O.P. Bruno, “Interpolated Factored Green Function” method for accelerated solution of scattering problems, *J. Comput. Phys.* 430 (2021) 110095.
- [12] J.-P. Berenger, A perfectly matched layer for the absorption of electromagnetic waves, *J. Comput. Phys.* 114 (1994) 185-200.
- [13] T. Betcke, N. Salles, and W. Śmigaj, Overresolving in the laplace domain for convolution quadrature methods, *SIAM J. Sci. Comput.* 39 (2017), pp. A188–A213.
- [14] O.P. Bruno, M. Lyon, C. Pérez-Arancibia, C. Turc, Windowed Green function method for layered-media scattering, *SIAM J. Appl. Math.* 76(5) (2016) 1871-1898.
- [15] O.P. Bruno, E. Garza, A Chebyshev-based rectangular-polar integral solver for scattering by general geometries described by non-overlapping patches, *J. Comput. Phys.* 421 (2020) 109740.
- [16] O.P. Bruno, E. Garza, C. Pérez-Arancibia, Windowed Green function method for nonuniform open-waveguide problems, *IEEE Trans. Antenn. Propag.* 65 (2017) 4684-4692.
- [17] O.P. Bruno, S. Lintner, A high-order integral solver for scalar problems of diffraction by screens and apertures in three-dimensional space, *J. Comput. Phys.* 252 (2013).
- [18] O.P. Bruno, S. Lintner, Second-kind integral solvers for TE and TM problems of diffraction by open arcs, *Radio Sci.* 47 (6) (2012).
- [19] O.P. Bruno, L. Kunyansky, A fast, high-order algorithm for the solution of surface scattering problems: Basic implementation, tests, and applications, *J. Comput. Phys.* 169 1 (2001) 80-110.
- [20] O.P. Bruno, M. Lyon, High-order unconditionally stable FC-AD solvers for general smooth domains I. Basic elements, *J. Comput. Phys.* 229 (6) (2010) 2009-2033.
- [21] O.P. Bruno, T. Yin, Regularized integral equation methods for the elastic scattering problems in three dimensions, *J. Comput. Phys.* 410 (2020) 109350.
- [22] O.P. Bruno, T. Yin, A windowed Green function method for elastic scattering problems on a half-space, *Comput. Methods Appl. Mech. Engrg.* 376 (2021) 113651.

- [23] Q. Chen, H. Haddar, A. Lechleiter, P. Monk, A sampling method for inverse scattering in the time domain, *Inverse Problems* 8 (2010) 85001-85017.
- [24] X. Chen, A. Friedman, Maxwell's equations in a periodic structure, *Transactions of the American Mathematical Society* 323 (1991) 465-507.
- [25] D. Colton and R. Kress, *Inverse Acoustic and Electromagnetic Scattering Theory*, Berlin, Springer, 1998.
- [26] M. Costabel, M. Dauge, R. Duduchava, Asymptotics without logarithmic terms for crack problems, *Commun. Partial Differ. Equ.* 28 (2003) 869-926.
- [27] J. Douglas, J.E. Santos, D. Sheen, L.S. Bennethum, Frequency domain treatment of one-dimensional scalar waves, *Math. Models Methods Appl. Sci.* 3 (1993) 171-194.
- [28] T. Ha-Duong, On retarded potential boundary integral equations and their discretisation, in *Topics in Computational Wave Propagation: Direct and Inverse Problems*, M. Ainsworth et al., eds., Springer Berlin Heidelberg, Berlin, Heidelberg, 2003, pp. 301–336.
- [29] B. Engquist, A. Majda, Absorbing boundary conditions for the numerical simulation of waves, *Math. Comp.* 31 (1977) 629–629.
- [30] L.C. Evans, *Partial Differential Equations* (2nd edition), Graduate Studies in Mathematics, Vol. 19, American Mathematical Society, Providence, 2010.
- [31] D.A. French, T.E. Peterson, A continuous space-time finite element method for the wave equation, *Math. Comp.* 65 (1996) 491-506.
- [32] M.J. Grote, A. Schneebeli, D. Schötzau, Dicontinuous Galerkin finite element method for the wave equation, *SIAM J. Numer. Anal.* 44 (2006) 2408-2431.
- [33] M. Hassell, T. Qiu, T. Sánchez-Vizuet, F.-J. Sayas, A new and improved analysis of the time domain boundary integral operators for acoustics, *J. Integral Equations Applications* 29(1) (2017) 107-136.
- [34] D.S. Jones, *The Theory of Electromagnetism*, Pergamon Press Oxford, 1964.
- [35] I. Labarca, R. Hiptmair, Acoustic scattering problems with convolution quadrature and the method of fundamental solutions, *Commun. Comput. Phys.* 30 (2021) 985-1008.
- [36] A.R. Laliena, F.-J. Sayas, Theoretical aspects of the application of convolution quadrature to scattering of acoustic waves, *Numer. Math.* 112 (2009) 637-678.
- [37] J.-F. Lee, R. Lee, A. Cangellaris, Time-domain finite-element methods, *IEEE Trans. Antenn. Propag.* 45 (1997) 430–442.
- [38] Y. Li, W. Zheng, X. Zhu, A CIP-FEM for high-frequency scattering problem with the truncated DtN boundary condition, *CSIAM Trans. Appl. Math.* 1(3) (2020) 530-560.
- [39] S. Lintner, O.P. Bruno, A generalized Calderón formula for open-arc diffraction problems: theoretical considerations, *Proceedings of the Royal Society of Edinburgh Section A: Mathematics* 145(2) (2015) 331-364.
- [40] Y. Liu, *Fast Multipole Boundary Element Method*, Cambridge University Press, New York, 2009.
- [41] C. Lubich, On the multistep time discretization of linear initial-boundary value problems and their boundary integral equations, *Numer. Math.* 67 (1994) 365-389.

- [42] R. C. MacCamy, Low frequency acoustic oscillations, *Q. Appl. Math.* 23 (1965) 247-255.
- [43] E. Mecocci, L. Misici, M. C. Recchioni, F. Zirilli, A new formalism for time-dependent wave scattering from a bounded obstacle, *J. Acoust. Soc. Am.* 107 (2000) 1825-1840.
- [44] A. Yilmaz, J.-M. Jin, E. Michielssen, Time domain adaptive integral method for surface integral equations, *IEEE Transactions on Antennas and Propagation*, 52 (2004), 2692–2708.
- [45] F.-J. Sayas, *Retarded Potentials and Time Domain Boundary Integral Equations*, Springer International Publishing, 2016.
- [46] E.P. Stephan, W.L. Wendland, An augmented Galerkin procedure for the boundary integral method applied to two-dimensional screen and crack problems, *Appl. Anal.* 3 (1984) 183-219.
- [47] J.A. Stratton, *Electromagnetic theory*, McGraw-Hill, New York, 1941.
- [48] A. Taflove, *Computational electrodynamics: the finite-difference time-domain method*, Artech House, Boston, 2000.
- [49] P. Werner, Low frequency asymptotics for the reduced wave equation in two-dimensional exterior spaces, *Math. Meth. Appl. Sci.* 8 (1986): 134-156.
- [50] Y. Xing, C.-S. Chou, C.-W. Shu, Energy conserving local discontinuous Galerkin methods for wave propagation problems, *Inverse Probl. Imag.* 7 (2013) 967-986.
- [51] X. Yuan, G. Bao, P. Li, An adaptive finite element DtN method for the open cavity scattering problems, *SIAM Trans. Appl. Math.* 12 (2020) 316-345.
- [52] Y. Yue, F. Ma, B. Chen, Time domain linear sampling method for inverse scattering problems with cracks, *E. Asian J. Appl. Math.* 12(1) (2022) 96-110.